Alma Mater Studiorum - Università di Bologna

SCUOLA DI SCIENZE

Dipartimento di Chimica Industriale "Toso Montanari"

Corso di Laurea Magistrale in

Chimica Industriale

Classe LM-71 - Scienze e Tecnologie della Chimica Industriale

Crystallization behaviour of poly(lactide) in immiscible blend with poly(ε-caprolactone), comparison with solution and melt-mixed blends

Tesi di laurea sperimentale

CANDIDATO

Greta Giacobazzi

RELATORE

Prof. Daniele Caretti

CORRELATORE

Prof. Alejandro J. Müller

Dott. Matteo Rizzuto

ABSTRACT

Poly(ε-caprolactone)-poly(carbonate) based copolymers, both block and random, were synthetized and characterized by ^{1}H-NMR spectroscopy. The copolymers have been tested as compatibilizers in 80/20 (w/w%) PLA/PCL blends prepared both by melt and solution mixing. The concentration of PCL-PC based copolymer added to the blends was 2 wt%. Compression moulded sheets and solvent cast films were evaluated by GPC (Gel Permeation Chromatography), TGA (Thermogravimetric Analysis), SEM (Scanning Electron Microscopy), PLOM (Polarized Light Optical Microscopy), DSC (Differential Scanning Calorimetry).

The addition of the copolymers does not cause an increased miscibility in PLA-PCL phases since a reduction of PCL particles size is not detected in SEM micrographs. At the same time, upon copolymers addition PLA's T_g value does not decrease in both melt and solution mixed blends.

Copolymers addition causes a reduction of molecular weight in melt mixed blends. In particular, the random copolymer (PCL-*ran*-PC) causes the highest reduction molecular weight in melt mixed blend, since it is characterized by the lower thermal stability as shown in TGA analysis. As result, PLA phase within melt mixed blends containing PCL-PC based copolymers shows a higher tendency to crystallize during both isothermal and non-isothermal DSC experiments. The increased crystallization of PLA phase is attributed to an increase in spherulitic growth kinetics determined by PLOM analysis. Upon molecular weight reduction in melt mixed blends containing copolymers, PLA chains have a higher mobility resulting in an improved motion towards the growing crystal front.

SUMMARY

1. INTRODUCTION

1.1. Crystallization of polymers

1.1.1. Background

The crystallization of polymers is a dynamic process associated with partial alignment of theirs molecular chains into ordered crystals. During crystallization, molecular chains that are in a highly disordered random state fold together and form ordered regions called lamellae.

In the melt state, polymers are long molecular chains which form irregular coils. In amorphous polymers such structure is retained upon cooling, whereas in crystalline polymers the chains rearrange upon freezing and form partly ordered regions.

However, also in crystalline polymers not all the chains can align forming a perfect crystal, but amorphous regions are included within crystalline domains (Figure 1.1).
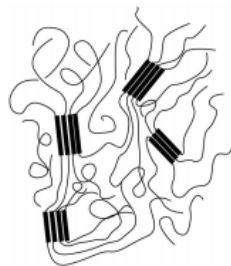
Figure 1.1: Schematic representation of ordered regions surrounded by the amorphous phase.

The tendency of a polymer to crystallize depends on its molecular structure: a constitutional, configurational and conformational regularity is required. At the same time, the type of crystal (size, number and structure) depends on several parameters, such as the molecular characteristics, composition, molecular weight and the processing conditions (like the crystallization temperature and cooling time).

Most of the properties of the polymer depend on the amount of crystalline phase.

For instance, in a crystalline polymer, the ordered area has a higher refractive index than the amorphous one, so crystalline polymers are usually opaque because of light scattering on the boundaries between one area to the other.

At the same time, also thermal stability, strength and rigidity of a polymer are influenced by its crystallinity, since in a crystalline structure the molecular chains are closely packed and thus are more organized to support thermal and mechanical stress.[1]

The degree of crystallinity is an important factor affecting the biodegradability of a polymer. Amorphous phase is more easily liable to enzymatic degradation since the molecules are loosely packed; on the other hand crystalline phase is much more resistant to enzymatic attack.[2]

1.1.2. Crystallization kinetic

The crystallization process consists of two consecutive phenomena: nucleation and crystal growth.

Nucleation of a crystal starts with the formation of small-sized areas where a group of molecular chains or their segments occur aligned. These seeds can either dissociate, if thermal motion destroys the molecular order, or grow further forming the crystal.

Since the alignment of chains occurs at low molecular mobility, the greater is the degree of supercooling from the melt state, the most favourable will be the formation of nuclei.[3]

Taking into account the site where the formation of nuclei starts in the amorphous phase, homogeneous and heterogeneous nucleation can be distinguished.

Homogeneous nucleation is a spontaneous process in which molecular chains occur parallel because of slow motion due to the supercooling. On the other hand, heterogeneous nucleation occurs at the surface of impurities, plasticizers, fillers and other additives present in the polymer matrix and, thus, a lower supercooling is required.[1]

Taking into account how the nuclei are formed, is it possible to distinguish two types of nucleation depending on the crystallization temperature: instantaneous and sporadic nucleation.

At low crystallization temperature (T_c) and thus high supercooling nucleation is instantaneous and many nuclei are formed at the same time. In this condition, a lot of crystals of small size are formed.

On the other hand, at high crystallization temperature (low supercooling), nucleation is sporadic and the formation of nuclei occurs at different time. In this case, few crystals of large size are formed, since the growth rate becomes higher than the nucleation one.[4]

Consecutive to nucleation is the crystal growth that is achieved by further addition of folded polymer chain segments. It only occurs at temperatures below the melting temperature (T_m) and above the glass-transition temperature (T_g). In proximity of T_m the molecular mobility is too high preventing the alignment of the chains whereas close to the T_g the melt-viscosity limits chains diffusion to the growth front.[1]

Figure 1.2 shows a comparison between nucleation rate (I) and crystal growth rate (G).[3] It can be appreciated that both the nucleation and the crystal growth exhibit a bell-shape trend with a maximum depending on crystallization temperature.
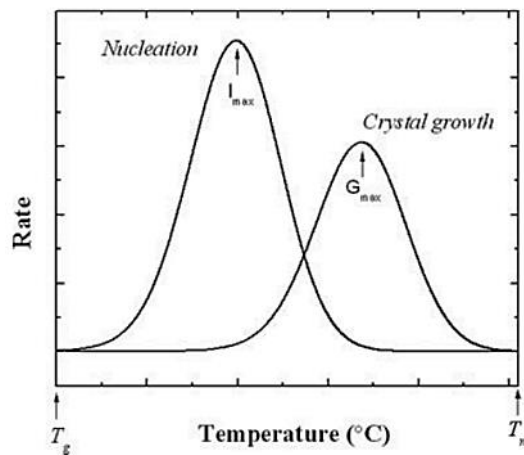
Figure 1.2: Schematic representation for the primary nucleation rate (I) and crystal growth rate (G) as a function of the isothermal crystallization temperature. Adapted from Lorenzo and Müller.[3]

As shown, nucleation is enhanced at higher supercooling since the alignment of chains occurs at low molecular mobility, whereas crystal growth is favoured at higher temperature being governed by the chains mobility to the growth front.

If the overall crystallization rate is determined by differential scanning calorimetry (DSC) the contribution of both nucleation rate and crystal growth rate are considered resulting in a bell-shaped trend as shown in Figure 1.3.

Figure 1.3: Overall crystallization rate as a function of temperature.

Values obtained from isothermal overall crystallization data are reported as the inverse of half-crystallization time ($1/t_{50\%}$) and consider both the nucleation rate and the crystal growth rate.

1.1.3. Avrami theory

Avrami theory allows describing the crystallization kinetics of polymeric materials.[5] Data obtained from isothermal crystallization experiments can be fitted by the Avrami equation which can be expresses by the following[6]:

$$1-V_c=\exp[-k(t-t_0)^n] \qquad\qquad \text{Eq.1.1}$$

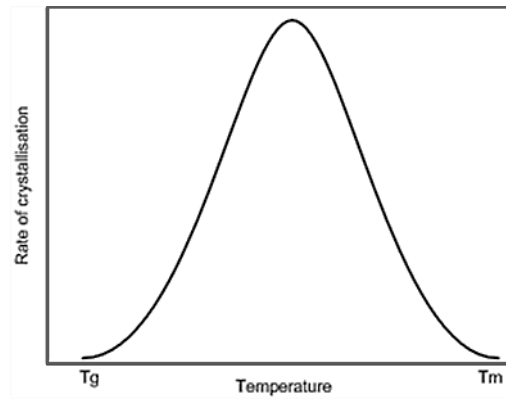Where t is the experimental time, t_0 is the induction time, V_c is the relative crystallinity volumetric fraction, k is the overall crystallization rate constant and n is the Avrami index value that is related to both nucleation and crystal growth. The Avrami index value gives information about how the nuclei are formed and the morphology of the crystals, being the results of these two contributions.

As previously explained nucleation may be instantaneous or sporadic. The contribution to the Avrami index value (n) is 0 when the nucleation is instantaneous whereas it is 1 when the nucleation is sporadic.

On the other hand, crystals formed during crystallization could have one, two or three dimension producing a contribution of 1, 2 or 3 respectively in the n value. By the sum of these two contributions the Avrami index value n is calculated.

The relative volume fraction crystallinity V_c is calculated according to Equation 1.2:

$$V_c = \frac{W_c}{W_c + \frac{\rho_c}{\rho_a}(1-W_c)}$$ Eq. 1.2

Where W_c is the relative crystallinity mass fraction, ρ_c is the density of fully crystalline material and ρ_a is the density of fully amorphous material.

The relative crystallinity mass fraction can be calculated by direct volume measurements or isothermal DSC experiments.

By isothermal DSC experimental, W_c is calculated according to the following equation:

$$W_c = \frac{\Delta H_{(t)}}{\Delta H_{TOT}}$$ Eq. 1.3

Where $\Delta H_{(t)}$ is the enthalpy value of crystallization as a function of crystallization time and ΔH_{TOT} is the enthalpy value after completion of the crystallization process.

Applying the logarithmic properties, the Avrami equation (Eq. 1.1) can be rearranged as follows:

$$\log[-\ln(1-V_c)] = \log(k) + n\log(t-t_0)$$ Eq. 1.4

Plotting $\log[-\ln(1-V_c)]$ as a function of $\log(t-t_0)$ the values of k and n can be obtained.

By the Avrami theory is possible to determine the half-crystallization time $1/t_{50\%}$ that is calculated by the following equation:

$$t_{50\%} = \left[-\frac{\ln[1-V_c]}{k}\right]^{1/n}$$ Eq. 1.5

1.2. PLA

1.2.1. Bioplastics

One of the fastest-growing materials sectors of the global plastic industry is the production of commodities from renewable resources, referred to as bioplastics.[7,8]

The main driver is the interest in reducing use of petroleum as a feedstock, under the pressure of its contribution to climate change, its pricing variability and its occasional role as a political weapon. By the way, the growth interest for bioplastics is connected to clear benefits for customers and environment, such as the consumer demand for more environmentally-sustainable products or the extra end-use benefits upon recent legislative development, as the "green tax" of Germany or the new environmental regulations in Japan.[9]

At the moment, mostly due to their high price level and low performance in comparison with conventional petrochemical counterparts, the number of competitive bioplastics is rather limited and only a few of them are both biodegradable and biobased.

Lignin and thermoplastic starch blends (TPS) have been received increasing attention as a source for value-added products but are still relatively underused.[10]

On the other hand, poly-lactic acid (PLA) and poly-hydroxyalkanoates (PHA) are well established biopolymers, commercially available, with a promise market increase.

1.2.2. PLA synthesis

Poly(lactic acid) (PLA) is a biobased, biodegradable and biocompatible aliphatic polyester widely used in biomedical field (i.e. sutures, clips, plates and screws or in drug delivery devices)[11] and in food packaging applications.[12,13]

The basic monomer of PLA is lactic acid (LA), also named 2-hydroxypropanoic acid. Lactic acid is chiral, consisting of two optical isomers. One is known as L-(+)-lactic acid and the other is D-(-)-lactic acid (Figure 1.4).

L-(+)-lactic acid   D-(-)-lactic acid

Figure 1.4: Optical isomers of lactic acid: L(+)-lactic acid and D-(-)-lactic acid.

The optical purity of lactic acid is a crucial parameter in PLA crystallization. As the optical purity of LA is lowered, the PLA capacity of crystallization decreases failing the configurational regularity.

Lactic acid is mainly produced with two methods: chemical synthesis from petrochemical feedstock and bacterial fermentation of carbohydrates.

The majority of the produced LA is obtained by bacterial fermentation of natural feedstocks.[14]

Starting from the lactic acid monomer, the synthesis of poly(lactic acid) can proceeds by two different routes of polymerization: direct polycondensation of the monomer and ring-opening polymerization through a cyclic intermediate named lactide.

From these two routes, derives a common misunderstanding in PLA nomenclature. Poly(lactic acid) refers to PLA obtained by polycondensation, poly(lactide) refers to PLA obtained by lactide intermediate.

Direct polycondensation of lactic acid involves the removal of water by condensation and allows obtaining only low molecular weight polymer, mainly because of the presence of water and impurities. One possible solution to increase its molecular weight is the use of chain extending or coupling reagents.

Although this process is the most economic route to obtain PLA, the presence of unreacted chain extending produces a drastic alteration of biodegradability.

Another possible solution to increase the molecular weight of PLA is the direct condensation of LA in solution in which water is continuously removed by the azeotropic distillation. Although high molecular weight can be achieved, this polymerization requires high concentration of catalyst that could cause degradation of the final product and toxicity.[15]

The most established method to obtain high molecular weight PLA is the ring-opening polymerization (ROP) through the lactide intermediate.[16] In this process, lactic acid is firstly polymerized to oligomers by removing water from the reaction

medium. In a second step, oligomers are catalytically depolymerized to form a cyclic intermediate dimer which is then purified. Finally, through ring opening polymerization, poly(lactide) is obtained.[17] (Figure 1.5)
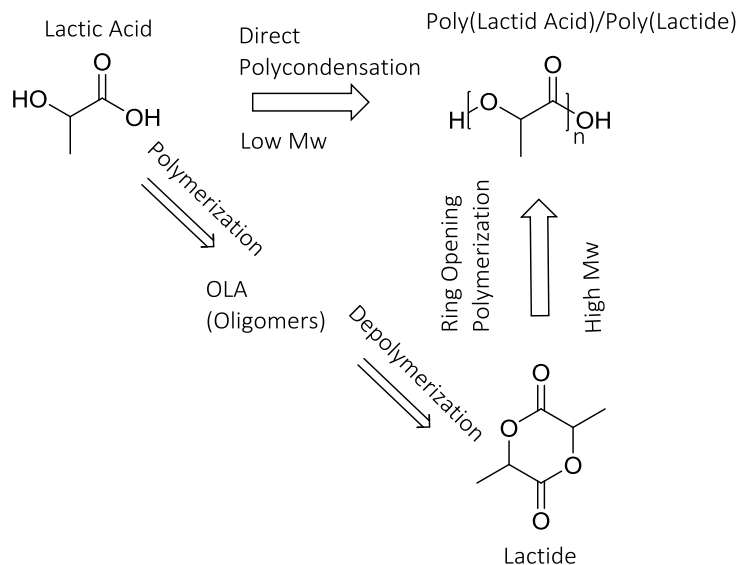
Figure 1.5: Schematic representation of PLA synthesis through direct polycondensation or ring opening polymerization.

Lactide exists in three different forms: D-lactide, L-lactide and meso-lactide (Figure 1.6). Only D-lactide and L-lactide are optically stereoisomers able to produce stereoregular PLA.
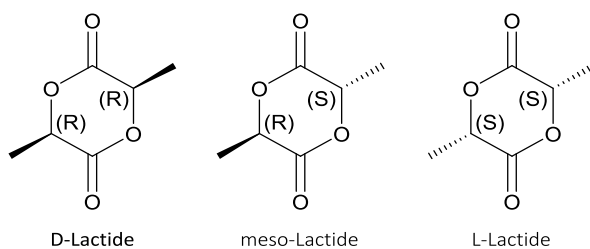
Figure 1.6: Different forms of lactide: D-lactide, meso-lactide and L-lactide.

The crystalline polymers coming from pure L- or pure D-lactide feed are referred to PLLA and PDLA respectively, the meso-PLA is obtained from DL-lactide while amorphous PDLLA is obtained from the random distribution of the D and L isomers in the macromolecular chains.[18]

Tin (II) octanoate ($Sn(Oct)_2$) is the most common catalyst used for lactide polymerization through ROP mechanism, thanks to its solubility properties, high

catalytic activity and ability to favour the formation of high molecular weight polymers ($\overline{M_W}$ above than 100.000) with low level of racemization (<1%).

Ring opening polymerization proceeds through a *coordination-insertion* mechanism shown in Figure 1.7. Molecular modelling suggests that two molecules of an alcohol (ROH) exchange with the octanoate to form tin (II) alkoxides (a). Subsequently, the insertion occurs in two steps which are a nucleophilic attack of the alkoxide on the monomer (b,c) followed by ring opening (d) and propagation (e).[19]
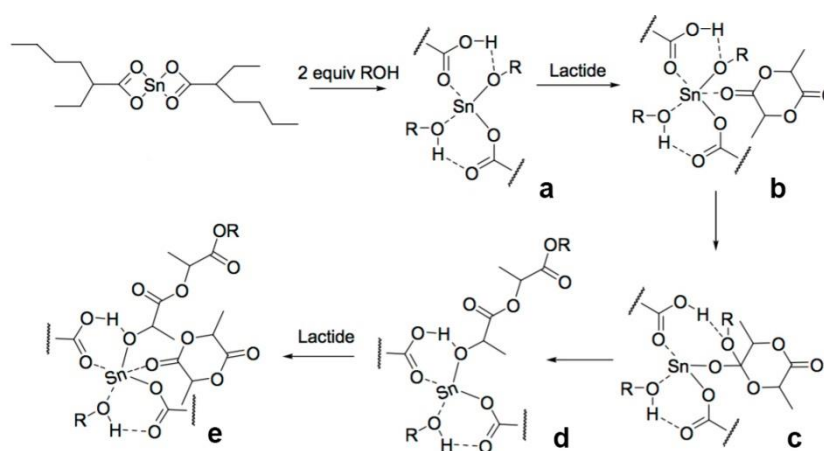
Figure 1.7: Coordination-insertion mechanism of Sn(Oct)$_2$ in catalyzed polymerization of L-lactide.

1.2.3. PLA properties

The physical properties of PLA, including melting temperature, degree of crystallization and mechanical properties but also degradation behaviour strongly depend on its molecular weight as on its stereochemical composition.[15]

PLLA homopolymer obtained from pure L-LA has an equilibrium crystalline melting point (T_{m0}) of 207 °C and a glass-transition temperature (T_g) about 60 °C. However, commercially available PLA usually shows a melting point of 170-180 °C due to the slight racemization, impurities and imperfect crystallites. Stereochemical defects reduce PLLA melting point and its extent of crystallization until a roughly 15% of defects incorporation which results in an amorphous polymer.[20]

Despite of PLA good mechanical properties, transparency and biodegradability, its very low impact strength value and its brittleness limit its applications.

One key factor in extending PLA usage derives from the control of its crystallization rate. Since in its amorphous form the range of application of PLA is severely limited by its low glass transition temperature, an increase of its crystallization speed is desired. At temperatures greater than PLA's T_g only the crystalline PLA phase can confer useful mechanical properties. Thus, the crystalline form is required to increase the temperature resistance of the material as well as to improve mechanical properties. However, PLA has a slow crystallization rate resulting in longer processing time if crystalline sample is desired.[21]

1.2.4. Thermal and hydrolytic degradation of PLA

Poly(lactic acid) is a degradable polyester susceptible to hydrolytic and thermal degradation.[22] At the same time, PLA is biodegradable, a characteristic that makes it particularly interesting for no durable applications, as biomedical use or food packaging.[23]

The chains scission at room temperature proceeds by hydrolysis of the ester linkages, promoted by moisture, heat or presence of residues (metal catalyst or unreacted monomers).[24]

At high temperature, PLA undergoes through thermal degradation. This process can be attributed to hydrolysis by trace amounts of water but also to (a) zipper-like depolymerisation, (b) oxidative random main-chain scission, (c) intermolecular transesterification to monomeric and oligomeric esters, and (d) intramolecular transesterification to monomer and oligomer lactides of low M_w.[25] Therefore a careful control of the processing conditions must be taken in order to conserve the final properties of the material (i.e., crystallization behaviour, mechanical and rheological properties).[26]

McNeill and Leiper proposed that above 200 °C PLA can degrade through a "backbiting" ester interchange reaction involving the -OH chain ends. Depending on the point in the backbone at which the reaction occurs, the product can be a lactide molecule, an oligomeric ring, or acetaldehyde and carbon monoxide.[27]

The formation of acetaldehyde is expected to increase with increasing processing temperature due to the increased rate of the degradation reactions.

The acetaldehyde generated during melt processing of PLA must be minimized if PLA has to be used for food packaging.[28]

At the same time, the formation of lactide due to depolymerization is undesirable since it causes the reduction of PLA melt viscosity and elasticity.
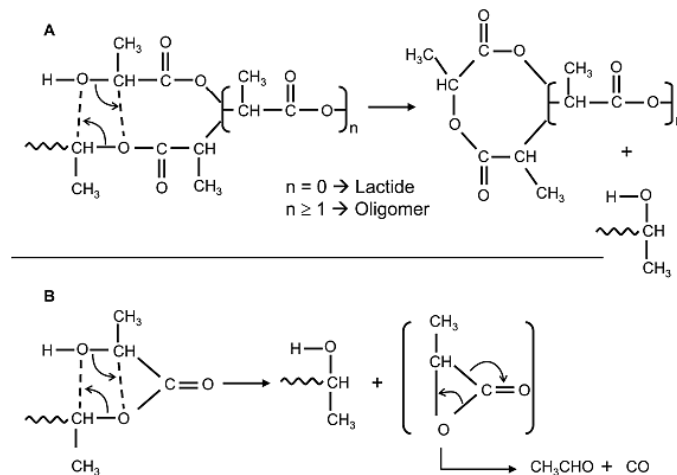
Figure 1.8: Thermal degradation of PLA. Adapted from McNeill and Leiper.[27]

1.2.5. PLA crystallization

A considerable amount of poly(lactic acid) properties depend on its degree of crystallinity. Therefore, the study of the PLA crystallization has tremendous relevance from both academic and industrial point of view.

Control of PLA crystallization kinetics is not a trivial issue, since it depends on the relative amount of the two stereoisomeric forms in which lactide exists (i.e., L- or D- lactide) and on its molecular weight. Only if one of the two forms is present in a high enough amount (at least more than 96–97%), PLA is able to develop significant crystallinity. At the same time, only if PLA has an adequate molecular weight can crystallize.

PLA is polymorphic, therefore, depending on crystallization conditions (i.e. crystallization temperature), different crystalline structures can be obtained. Indeed crystallization at temperature above 120 °C, from melt or solution, results in the most common and stable crystal type: the α-form. This structure consists in two antiparallel 10_3 helical chain segments packed in an orthorhombic unit cell with 3.3 monomers per turn and a length of the repeating unit of 27.8 nm.

At temperature below 120 °C, α-form can be replaced by pseudohexagonal α'-form. In this case the molecule segments have the same 10_3 helical chains

conformation adopted in α-form but with higher conformational disorder and lower packing density.

More recent studies demonstrate that the α'-form crystal is preferentially formed only at crystallization temperatures below 100 °C, while in the temperature range of 100-120 °C both α and α'-form can arise.[29]

The existence of the two different crystal forms is responsible of the particular thermal behaviour. In PLA crystallized at temperatures corresponding to α'-form crystal formation, a small exotherm appears just before the single melting peak, due to the transformation of disordered α'-form to the ordered α-form crystals. On the other hand, when PLA is crystallized at temperature of the two crystals forms coexistence, a double melting peak appears.[30]

Additional crystals form can be obtained under special processing condition. Hot-drawing melt-spun or solution-spun PLA fibres lead to β-form crystals. β-form crystals whose melting temperature is 10 °C lower than the melting temperature of the corresponding α-form, have an orthorhombic unit cell with six chains in the helical conformation.

At the same time, γ-form crystals are obtained by epitaxial crystallization of PLA in hexamethylbenzene. This crystal structure is characterized by two antiparallel helices in an orthorhombic unit cell.[31]

1.3. Crystallization of PLA phase within miscible and immiscible blends

The crystallization of a polymer takes place in a defined temperature range, between the values of the glass transition temperature, T_g, and the equilibrium melting temperature of the crystallizable polymer, T_{m0}. Below T_g the chain mobility is inhibited, while at temperatures near T_{m0} the crystal nucleation does not occur. In a polymer blend the relative position of T_m and T_g depends on the miscibility between the components. Depending on the favourable specific interaction between the polymeric counterparts, a miscible or an immiscible blend may be obtained.

In a miscible blend, a single-phase system, which combines the properties of the components, is formed. Therefore, the tendency to crystallize of one component

can either increase or decrease, depending on the changes of the glass transition and equilibrium melting temperature produced by blending.

In the case that a crystallizable component is blended with a lower T_g miscible counterparts, its chain mobility during crystallization is higher than before blending, which facilitates the chain motion in the melt towards the growing crystal fronts and the further arrangement of the otherwise stiff chains into the crystals, providing a positive contribution to the spherulitic growth rate.

Typical miscible blends of PLA mixed with low T_g components are: PLA/poly(ethylene oxide) (PLA/PEO) and PLA/poly(ethylene glycol) (PLA/PEG) blends. In this case the single T_g of the blends is lower than that of neat PLA, and the spherulitic growth rate increases with increasing composition of the lower T_g polymer counterpart.[32]

However, because of the small mixing entropy contribution, the polymer pairs are generally not miscible in each other and thus almost all of the commercial blends are immiscible. In this case, the crystallization becomes much more complicated to the effects of phase separation and interface.

Although, the crystallization of each component takes place in domains separated from the other and at temperatures that are almost near the characteristic crystallization temperatures of the neat polymers, large changes can be observed, depending on the degree of dispersion of the minor phase into the matrix, with appearance of fractionated or retarded crystallization phenomena.

The fractionation of crystallization may be observed when the crystallizable component constitutes the dispersed phase, depending on its dispersion degree. At the same time, changes in the primary nucleation density and nucleating activity may also be found due to the occurrence of migration of heterogeneities between the phases in the melt when the interfacial free energy of the impurities within their melt phase is higher than the interfacial energy of those impurities within the other melt phase of the blend. Moreover, changes in the heterogeneous nucleation of a crystallizable component in an immiscible blend may occur due to the effect of surface nucleation at the interface between the phases.[33]

For instance, Tsuji *et al.*[34] reported that biodegradable poly(glycolic acid) accelerated the overall crystallization of PLLA during both the heating and

cooling processes as a polymeric nucleating agent. Zhou *et al.*[35] reported that poly(L-lactide)-b-poly(butyleneterephthalate)-b-poly(L-lactide) (PLA-b-PBT-b-PLA) tri-block copolymer was a potential polymeric nucleating agent for the crystallization of PLLA, as the nucleation density of PLLA spherulites was obviously increased in the presence of 5 wt% of PLA-b-PBT-b-PLA. Pan *et al.*[36] reported that the melt and cold crystallization behaviours of PLLA were accelerated by its blending with poly(vinylidene fluoride) in their immiscible polymer blends, and the enhanced crystallization of PLLA was attributed to the heterogeneously epitaxial and interface-assisted nucleation mechanism. Guo *et al.*[37] found that polyoxymethylene may act as a polymeric nucleating agent for the crystallization of PLLA.

1.4. Poly(lactide) (PLA)/Poly(ε-caprolactone) blends

One of the most extensively used way to improve PLA properties is the physical blending with other polymers. The properties of the resulting polymer blend are tuneable through the choice of blending components and their relative percentage amount.[38]

Poly(L-lactide)/poly(ε-caprolactone) blend has been extensively investigated due to the biodegradability and mechanical properties of the obtained system.

Poly(ε-caprolactone) is a biodegradable and semicrystalline polyester with a low melting point of around 60 °C and a low glass transition temperature of about -60 °C.[39] At room temperature PCL shows low tensile modulus and high elongation at break while PLA presents high Young modulus and low elongation at break.

As result, PCL flexibility can compensate PLA brittleness improving its mechanical properties and applications. Although the solubility parameters of PLA and PCL are quite close (i.e., 10.1 (cal/cm^3)$^{1/2}$ for PLA and 9.2 (cal/cm^3)$^{1/2}$ for PCL) there are not specific interaction between the polymer chains that can induce phases miscibility.[40] Therefore, the two polyesters are immiscible over a wide range of composition, temperature and molecular weight both when they are melt mixed and solution mixed.

Several methods have been employed to enhance the miscibility between PLA and PCL phases. These include the addition of copolymers, the addition of

reactive polymers with functional groups and the addition of low molecular weight chemicals.

1.5. Compatibilizers

In PLA/PCL blends several strategies of compatibilization have been followed in order to improve the miscibility between the two phases.[41]

Compatibilization allows to a size reduction of the dispersed phase through the reduction of interfacial tension and prevents the coalescence of the dispersed phase stabilizing the formed phase morphology.

The addition of block copolymers is an efficient way to compatibilize polymer blends due to their efficiency to form entanglements with the corresponding phases and their relative low cost in comparison with the other methods of compatibilization.[42]

Many efforts have been focused on the compatibilization of PLA/PCL blends through the addition of block copolymers of PLA and PCL. Exploiting this kind of copolymers, it is improved the interfacial adhesion between the phases causing a reduction of the dispersed phase size. For instance, Wu *et al.*[43] reported a reduction from 10-15 µm to about 3-4 µm of PCL particle domains within a 70/30 PLA/PCL blend, using a PLA-PCL-PLA triblock copolymer as compatibilizer.

Effective results have been obtained also by using copolymers in which one of the two blocks is miscible, but not identical, to one of the blend component. Na *et al.*[44] have extended this approach to block copolymers in which one is PCL while the other one in miscible with PLA. They employed PEG-*b*-PCL block copolymer to compatibilize PLA/PCL blends and achieve improved mechanical properties upon copolymer addition.

Exploiting the same strategy, Rizzuto *et al.*[45] reported a threefold reduction of PCL particle size in 80/20 PLA/PCL blend by using a diblock copolymer of PLA and PC (miscible with PCL phase).

Also random copolymers are effective as compatibilizer, since the sequential comonomer units can be regarded as short block, miscible with the corresponding blend components. For instance, Choi *et al.*[46] reported a reduction from 10 µm to 3 µm of PCL domains within a 70/30 PLA/PCL upon the addition of the random copolymer PLA-*co*-PCL at 5%.

2. OBJECTIVE OF THE THESIS

Poly(lactide) is one of the most promising substitutes for petroleum based polymers, since it is at the same time bio-based, biocompatible and biodegradable. However, its drawbacks (i.e., slow crystallization rate, low T_g value, low toughness) are limiting its applications and commercial expansion.

One possible solution to improve PLA properties is its blending with another polymer counterpart. In this context, poly(ε-caprolactone) (PCL) is one of the best candidate, being flexible, biodegradable and biocompatible and thus allowing to achieve toughening of PLA without interfering with original applications.

At the same time, upon blending with PCL, PLA crystallization rate could be increased. However, the matter is not a trivial issue since it is dependent on more factors, as the preparation method of the blend and the miscibility between the phases.

In a miscible blend, a single phase system which combines the properties of the neat components is obtained. Therefore, the tendency to crystallize of one component can either increase or decrease, depending on the changes of the glass transition and equilibrium melting temperature expected upon blending.

In an immiscible blend, a multiphase system is obtained, whose crystallization rate of each component is strictly related to phase morphology and thus processing conditions, molecular characteristics, and interfacial properties of the blend.

The solubility parameters of PLA and PCL are quite close (i.e., 10.1 $(cal/cm^3)^{1/2}$ for PLA vs. 9.2 $(cal/cm^3)^{1/2}$ for PCL)[47], however there are not favourable interactions accounting for their miscibility. As a result, the two polymers are immiscible over a wide range of temperature, composition and molecular weight, as confirmed by many previous studies where the polymers were mixed in solution[48–50] or in the melt.[51–54]

A large effort has been devoted to improve PLA-PCL miscibility. Different kinds of compatibilizers have been proposed, including random copolymers and block copolymers, as well as reactive compatibilization/mixing.

In this work, a detailed investigation into the crystallization behaviour of PLA phase, within 80/20 PLA/PCL immiscible blends, has been carried out under

both non-isothermal and isothermal conditions. The compatibilizer effect of PCL-PC based copolymers, both block (PCL-*b*-PC) and random (PCL-*ran*-PC), has been tested. Particular emphasis has been focused on the morphology, crystallization and thermal properties of the blends upon copolymers additions.

At the same time, the influence of the processing condition on the morphology of the blend, and thus its crystallization behaviour, has been investigated by preparing the samples by both solution and melt blending.

In the following text, synthesis and characterization of PCL-PC based copolymers will be firstly presented. Secondarily, the effect of the copolymers on PLA/PCL blends, prepared by both solution and melt blending, will be analysed by taking a particular emphasis on the crystallization behaviour of PLA phase.

3. EXPERIMENTALS

3.1. Materials and methods

Poly(L-lactide) (PLA, Ingeo index: 4032D, 1.2-1.6 % D-LA isomer, $\overline{M_W}$ = 180 kDa) was purchased from NatureWorks[TM]. Before processing it was dried overnight under vacuum at 60 °C to avoid degradation reactions induced by moisture. Poly(ε-caprolactone) (PCL, Capa[TM] 6800, $\overline{M_W}$ = 87 KDa) was purchased from Perstorp and was used as received. Poly(carbonate) (PC, TARFLON® IV1900R) was purchased from Idemitsu Chemicals Europe and was used as received. ε-caprolactone (Sigma-Aldrich-CAS Number: 502-44-3) and tin octanoate (Sigma Aldrich-CAS Number: 301-10-0) were used as received.

Two different copolymers of poly(ε-caprolactone)-poly(carbonate) with a mass composition of 50/50 (w/w%) were used. These copolymers differ in their structure: PCL-*b*-PC is a multiblock copolymer and PCL-*ran*-PC is a random copolymer. Both copolymers were synthetized by ring opening polymerization using tin (II) octanoate as catalyst and toluene as solvent. The detailed synthesis is described in section 3.2.

Table 3.1: Molecular characteristics of copolymers. Composition (PCL content w/w%), PC and PCL units length, average molecular weight ($\overline{M_w}$), polydispersity (D) and glass transition temperature (T_g).

Sample	Comp. PCL[a] (w/w%)	PC length[b]	PCL length[b]	$\overline{M_w}$ (Da)[c]	D[d]	T_g (°C)[e]
PCL-*b*-PC	49	3	35	18500	1.4	-36
PCL-*ran*-PC	61	1	10	14600	2.3	-32

[a] Composition weight ratio between PCL and PC components determined by ^{1}H-NMR. [b] Length of PC and PCL units determined by ^{1}H-NMR. [c] Determined by GPC. [d] Determined as $\overline{M_w}/\overline{M_n}$. [e] Determined by DSC, heating curves at 10 °C/min.

3.2. Synthesis of PCL-PC based copolymers

- **Poly(ε-caprolactone)-*b*-Poly(carbonate) (PCL-*b*-PC)**

PCL-*b*-PC copolymer was synthetized in a 50/50 w/w% composition by a bulk ring opening polymerization using commercial ε-caprolactone and poly(carbonate). A schematic representation of the reaction is shown in Figure 3.1.

In order to exploit the miscibility of poly(carbonate) in ε-caprolactone a feeding ratio of poly(carbonate)/ε-caprolactone 33/67% was used.

In a three-neck flask 10 g of poly(carbonate) were weighted and, under nitrogen atmosphere, 20 mL of ε-caprolactone were added. The mixture was stirred under nitrogen flux until complete dissolution of poly(carbonate). Maintaining inert atmosphere, 3 mL of $Sn(Oct)_2$ (5 mol catalyst/mol monomer%) and 35 mL of toluene were added. The reaction mixture was immersed in an oil bath at 120 °C for 2 hours under stirring to allow the polymerization.

The raw products were dissolved in 50 mL of dichloromethane and then poured into 400 mL of methanol. The precipitate collected by filtration was purified by a reprecipitation with dichloromethane and methanol and finally dried through a vacuum pump.

- **Poly(ε-caprolactone)-*ran*-Poly(carbonate) (PCL-*ran*-PC)**

PCL-*ran*-PC copolymer was synthetized reproducing the same steps as in the synthesis of PCL-*b*-PC. The two syntheses differ only in the time of reaction and the modality of adding the monomer.

For the synthesis of PCL-*ran*-PC copolymer, 10 g of poly(carbonate) were weighted in a three-neck flask and, under nitrogen atmosphere, 10 mL of ε-caprolactone, were added. Maintaining inert atmosphere, 3 mL of $Sn(Oct)_2$ (5 mol catalyst/mol monomer%) and 35 mL of toluene were added. The reaction mixture was immersed in an oil bath at 120 °C. After 2 and 4 hours, 5 and 5 mL of ε-caprolactone were added for a total of 20 mL of the monomer. To allow the polymerization the reaction mixture is reacted for 12 hours.
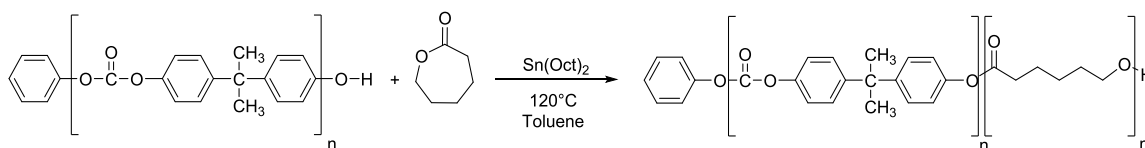

Figure 3.1: Schematic representation of copolymers synthesis.

3.3. Blends preparation

A constant PLA/PCL weight ratio of 80/20 was employed. Block and random copolymers were used as compatibilizer by adding 10% with respect to PCL phase. The composition of the final blends is approximately 80/20/2 PLA/PCL/PCL-*co*-PC. Table 3.2 reports the composition of the prepared blends.

Table 3.2: Composition of the prepared blends.

Sample name	PLA (w/w%)	PCL (w/w%)	PCL-*b*-PC (w/w%)	PCL-*ran*-PC (w/w%)
PLA (m)	100	-	-	-
PLA (s)	100	-	-	-
PCL (m)	-	100	-	-
PCL (s)	-	100	-	-
PLA/PCL (m)	80	20	-	-
PLA/PCL (s)	80	20	-	-
PLA/PCL/PCL-*b*-PC (m)	79	19	2	-
PLA/PCL/PCL-*b*-PC (s)	79	19	2	-
PLA/PCL/PCL-*ran*-PC (m)	79	19	-	2
PLA/PCL/PCL-*ran*-PC (s)	79	19	-	2

The blends were prepared by both solution and melt mixing. The ones prepared by solution mixing have been designated with: (s) while the corresponding ones prepared by melt blending have been designated with: (m).

In the first case, PLA, PCL and PCL-PC based copolymers were dissolved in dichloromethane at the concentration of 1 g/dL and stirred at room temperature for 3 hours. The solutions were casted in Petri dishes (diameter = 5 cm) obtaining films that were dried for 24 hours at room temperature and for another 24 hours at 60 °C under vacuum in order to remove any solvent residue.

In the second case, neat homopolymers and the PCL-PC based copolymers were melted and blended in a Collin twin-screw extruder (Teachline, L/D ratio 18, screw diameter 25 mm). Melt blending was performed at a screw speed of 200 rpm, a temperature of 200 °C with a residence time of approximately 1 minute. The extruded filaments were quenched in a water bath and pelletized. The pellets were dried overnight at 60 °C under vacuum and were compression moulded in a Collin P-200-E compression moulding machine at 200 °C (3 minutes without pressure followed by 3 minutes at 100 bar). Tensile testing

specimens (ASTM D 638 type IV, average thickness 1.84 mm) of the blends were obtained.

3.4. Spectroscopic analysis

Commercial poly(carbonate) and the synthetized copolymers were analysed by ^{1}H-NMR experiments. ^{1}H-NMR spectra have been recorded with a spectrometer Varian "Mercury 400" operating at 400 MHz on samples prepared in $CDCl_3$ at the 1.0 wt%. Chemical shifts (δ) for ^{1}H are given in ppm relative to the know signal of the internal reference (TMS).

3.5. Molecular weight analysis

Block and random copolymers and all the prepared blends were analysed by Gel Permeation Chromatography (GPC).

The samples were analysed by a Waters column with 717 Autosampler equipped with a double detector: Waters 2487 Dual λ Absorbance Detector and Waters 2410 Refractive Index Detector. The column works at 35 °C using THF as eluent. The samples were prepared at a concentration of about 0.07-0.10 (%w/V) weighting 3.5-5 mg that have been dissolved in 5 mL of THF.

3.6. Morphological analysis

The morphology of the blends was investigated by Scanning Electron Microscopy (SEM).

The tensile test specimens and the films were cryogenically fractured after 3 hours of immersion in liquid nitrogen. Fracture surfaces were observed after gold coating under vacuum, using a Zeiss EP EVO 50 electron microscope equipped with a EDS detector classifiable as Oxford Instrument INCA ENERGY 350 [z>4 (Be), resolution 133eV (MnKa @ 2500cps)].

Micrographs of the most representative inner regions of the specimens were obtained. PCL droplet diameters were measured on at least 100 particles. Number (d_n) and volume (d_v) average diameters and particles size polydispersity (D_p) were calculated by the following equations.

$$d_n = \frac{\sum_{i=1}^{n} n_i d_i}{\sum_{i=1}^{n} n_i} \qquad \text{Eq. 3.1}$$

$$d_v = \frac{\sum_{i=1}^{n} n_i d_i^4}{\sum_{i=1}^{n} n_i d_i^3} \qquad \text{Eq. 3.2}$$

$$D_p = \frac{d_v}{d_n} \qquad \text{Eq.3.3}$$

where n_i is the number of droplets 'i' of diameter d_i.

Polarized Light Optical Microscopy (PLOM) was employed to observe the morphology and growth kinetics of PLA spherulites. Micrographs were recorded by a LEICA DC 420 camera on film samples with a thickness of approximately 10 µm, cut from solvent casted films and tensile test specimens. By using a METTLER FP35Hz hot stage, the samples were firstly heated at 200 °C and held at this temperature for 3 minutes to erase previous thermal histories, and then they were cooled to the crystallization temperature and the isothermal spherulitic growth was followed by PLOM.

3.7. Thermal analysis

The copolymers and all the blends were analysed by Thermogravimetric analysis (TGA) and Differential Scanning Calorimetry (DSC).

The thermal stability of the blends was studied by TGA using a thermobalance TA Instruments, model TGAQ500. All measurements were performed under nitrogen atmosphere and using sample masses of approximately 7 mg. All the samples were heated from 40 to 600 °C at a rate of 10 °C/min.

The thermal behaviour of the blends was studied by DSC using a Perkin Elmer DSC Pyris 1 calorimeter equipped with a refrigerated cooling system Intracooler 2P calibrated with indium. All measurements were performed under nitrogen atmosphere and using sample masses of approximately 5 mg. The analyses were conducted with different methods as a function of the experiments.

In non-isothermal analyses, the copolymers were heated from 25 °C to 200 °C at the rate of 10 °C/min and held at 200 °C for 3 minutes to erase the thermal history. Then they were cooled at 10 °C/min until -80 °C (in order to see the glass transition temperature) and finally heated at 10 °C/min to 200 °C.

On the other hand, the blends were heated from 25 °C to 200 °C at the rate of 10 °C/min and held at 200 °C for 3 minutes to erase the thermal history. Then they were cooled at 10 °C/min until -20 °C and finally heated at 10 °C/min to 200 °C.

In isothermal analyses, the samples were heated from 25 °C to 200 °C at 20 °C/min and held at this temperature for 3 minutes to erase the thermal history. Then they were cooled at 60 °C/min (in order to avoid PLA crystallization during cooling) to the chosen isothermal crystallization temperature (T_c) and held at this temperature for 30 minutes while recording the evolved crystallization enthalpy. The isothermal crystallization temperature range was determined by preliminary tests to ensure that no crystallization occurred during the cooling step.

4. RESULTS AND DISCUSSION

4.1. Synthesis of PCL-PC based copolymers

4.1.1. Introduction

PCL-PC based copolymers have been synthesized under a precise structure design, upon careful screening of the reaction parameters. A PCL-PC symmetric composition (50/50 w/w%) is desired, in order to maximize the entanglements of each block with both the PLA and PCL phases. At the same time, the copolymers must have an adequate molecular weight to reduce the preferential migration into only one of the blend phases.

The synthesis has been carried out by bulk ring-opening polymerization (ROP), using ε-caprolactone and pre-synthetized poly(carbonate) as building blocks and exploiting the solubility of poly(carbonate) in ε-caprolactone.

This method is more suitable than the others present in literature (condensation between two suitably functionalized polymer chains, reactive blending of two homopolymers through exchange reactions and chemical modification with postpolymerization)[55] in the case that particular emphasis is focused on the final structure of the designed copolymer. In other words, only by ring-opening polymerization is possible to tune the reaction conditions in order to obtain both random and blocks copolymers and, at the same time, achieve a good control on the composition and molecular weight of the resulting polymer.

The reaction proceeds through $Sn(Oct)_2$-catalyzed polymerization of ε-caprolactone onto pre-synthetized poly(carbonate) blocks, instead of the *in situ* polymerization of both monomers. This is because the formation of poly(ε-caprolactone) and poly(carbonate) proceeds at different conditions and therefore is not achievable by a *one pot* reaction.

The mechanism for a ROP is a three step coordination-insertion mechanism.[56] It proceeds through the coordination of a protic reagents such as alcohols with $Sn(Oct)_2$ to form tin (II) alkoxides. Subsequently, the insertion occurs in two steps which are a nucleophilic attack of the alkoxide on the monomer followed by ring opening (Figure 4.1).
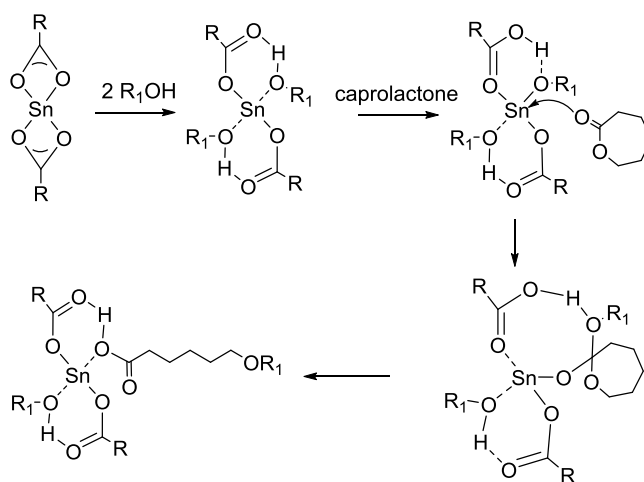
Figure 4.1: Mechanism for the Sn(Oct)$_2$ –Catalyzed ROP of ε-caprolactone.

In the synthesis of the PCL-PC based copolymers, the protic reagent that reacts with Sn(Oct)$_2$ is the final hydroxyl group of the poly(carbonate) chain. After the coordination step with formation of tin (II) alkoxide, ε-caprolactone insertion occurs, allowing the polymerization of ε-caprolactone from poly(carbonate) as shown in Figure 4.2.

Figure 4.2: Polymerization reaction of ε-caprolactone from preformed poly(carbonate).

During the polymerization of ε-caprolactone, transesterification between the growing chain of poly(ε-caprolactone) and carbonate can take place.

Figure 4.3: The transesterification reaction between the growing chain of poly(ε-caprolactone) and the poly(carbonate) chains.

This secondary reaction leads to a break in the poly(carbonate) chain with subsequent insertion of a poly(ε-caprolactone) block as shown in Figure 4.3.

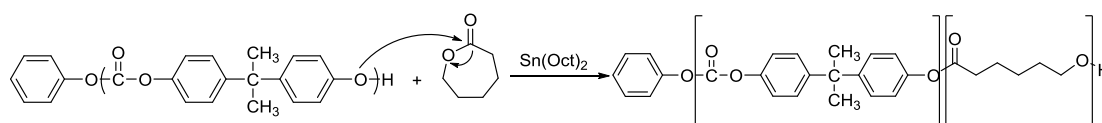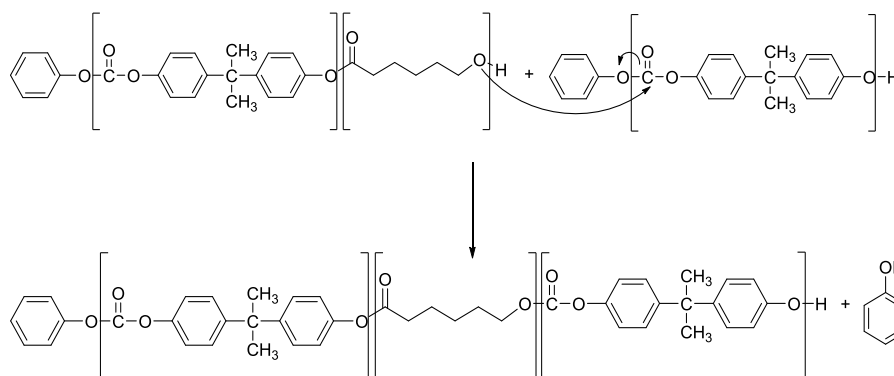The relative kinetics of both polymerization-transesterification reaction rates must be controlled as a function of the type of desired copolymer design (i.e., random or block).

On one hand, if block copolymer is wanted, transesterification reaction must be avoided, since it induce a shortening of the subsequent blocks of poly(ε-caprolactone) and poly(carbonate). Therefore, the polymerization reaction rate must be enhanced over the transesterification reaction rate.

On the other hand, if random copolymer is wanted, only transesterification can lead to the formation of short sequential comonomer units. Therefore, the transesterification reaction rate must be enhanced over polymerization reaction rate.

4.1.2. Reaction screening

The reaction conditions were optimized by a temperature, catalyst amount and time screening. In all the reactions a fixed poly(carbonate)/ε-caprolactone 33/67 w/w% ratio in the feeding was used, in this way it is possible to exploit the miscibility of poly(carbonate) in ε-caprolactone and, therefore, it is possible to carry out the reaction in bulk, with a general advantage of the polymerization rate and process condition.

Table 4.1: Reactions screening of catalyst amount, temperature, time for PCL-*co*-PC copolymer. Conversion of ε-caprolactone, composition of poly(ε-caprolactone) in the copolymers and length of poly(carbonate) and poly(ε-caprolactone) units were obtained by ^{1}H-NMR.

Sample	Cat. (mol/mol%)	Temp. (°C)	Time (h)	Solv. (mL)	Conv. CL (%)	Comp. (PCL w/w%)	PC length	PCL length
1	5	100	4	10	42	14	14	47
2	5	120	4	10	71	52	4	34
3	1	120	16	5	89	64	2	16
4	5	120	16	5	91	55	2	27
5	5	120	1	5	37	31	6	32
6	5	120	2	5	67	47	4	31
7	5	120	3	5	79	54	4	35
8	5	120	4	5	79	53	3	26
9	5	120	16	5	91	55	2	27

- Temperature screening

Samples 1 and 2 differ only for the temperature used (i.e.; 100 and 120 °C). To an increase of temperature corresponds an increase in ε-caprolactone conversion. As result, at 100 °C a 14/86 poly(ε-caprolactone)/poly(carbonate) composition is obtained, whereas at 120 °C the composition of 52/48 is reached. Therefore 120 °C has been chosen as the right temperature for the following tests.

- Catalyst quantity screening

Samples 3 and 4 were both obtained at 120 °C and differ only for the amount of catalyst used (i.e.; 1% and 5% respect to ε-caprolactone feed). The amount of catalyst doesn't affect the copolymer composition but its structure. Upon 1% of catalyst the poly(carbonate) transesterification rate is higher than the polymerization rate of ε-caprolactone. As result poly(carbonate) and poly(ε-caprolactone) blocks are shorter. On the other hand, upon 5% of catalyst the polymerization rate is enhanced and therefore longer blocks are obtained.

- Time screening

Samples from 5 to 9 were conducted at an increasing polymerization time from 1 to 16 hours. At 1 hour blocks composed of 6 and 32 units of PC and PCL respectively were obtained, however, without reaching the desired composition of 50/50 PCL/PC. This is reached after 2 hours of reaction and the poly(carbonate) block consists of 4 units because transesterification takes place as shown by the sample 6. After 4 hours of reactions (sample 8) the composition doesn't significantly change but the length of both blocks decreases until 2/27 PC/PCL after 16 hours of reaction (sample 9). The length of the PCL block seems to be smaller because it's calculated as the average of the blocks forming the chain.

4.1.3. Synthesis

After screening, reaction conditions were selected in order to obtain a random and a block copolymer with a mass composition equal to 50:50 of PC:PCL. For the block copolymer, the temperature of 120 °C, the 5% of catalyst and the time of 2 hours were selected as shown in Table 4.2, in order to reproduce the

sample 6. As reported in Table 4.2, a composition close to 50:50 was achieved and the lengths of the constituent blocks are 3/35 PC/PCL.

On the other hand, the random copolymer was obtained setting 120 °C, a 5% catalyst and 12 hours of reaction. The main difference compared to other reactions is that the monomer has been introduced into the reaction medium by subsequent additions. This system was chosen in order to improve transesterification reaction rather than polymerization avoiding a longer poly(ε-caprolactone) block. In the same way, the transesterification reaction is improved by long reactions time as demonstrated by the previous sample 9. In fact, setting 12 hours as reaction time the block of poly(carbonate) is reduced to 1 unit as shown in Table 4.2.

Table 4.2: Reaction conditions to obtain PCL-*b*-PC and PCL-*ran*-PC copolymers. Conversion of ε-caprolactone, composition of poly(ε-caprolactone) in the copolymers and length of poly(carbonate) and poly(ε-caprolactone) units determined by ^{1}H-NMR.

Sample	Cat. (mol/mol%)	Temp. (°C)	Time (h)	Solv. (mL)	Conv. CL (%)	Comp. (PCL w/w%)	PC length	PCL length
PCL-*b*-PC	5	120	2	35	98	49	3	35
PCL-*ran*-PC	5	120	12	35	75	61	1	10

4.2. Characterization of PCL-PC based copolymers

4.2.1. Spectroscopic characterization

Poly(ε-caprolactone)-poly(carbonate) based copolymers were characterized by ^{1}H-NMR, using the work of Cayuela *et al.* as reference.[57] A preliminary ^{1}H-NMR spectrum of poly(carbonate) was registered (Figure 4.4). The signals observed at 7.25, 7.17 and 1.68 ppm are assigned respectively to protons **A**, **B** and **C** present in the main chain of poly(carbonate), whereas the signals at 6.70 and 7.40 ppm correspond respectively to proton $\mathbf{A_2}$ (phenolic end group) and $\mathbf{B_1}$ (phenylic end group).

The average number of repeating units of PC chain ($\bar{n}$), has been calculated considering the ratio between signals of proton in the chain/end groups.
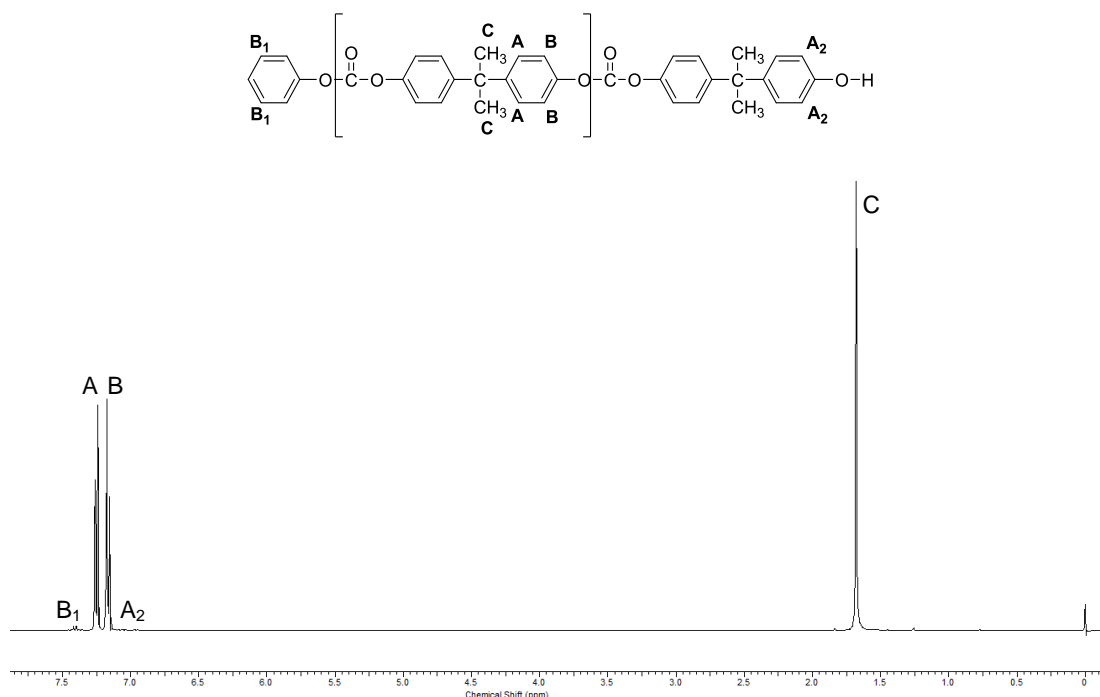
Figure 4.4: ^{1}H-NMR spectrum of poly(carbonate).

The following formula has been used:

$$\bar{n} = 2 \times \frac{I(C)/6}{(I(B_1) + I(A_2))/2} = 33 \qquad \text{Eq. 4.1}$$

where I(C) corresponds to the integral value of protons **C** representing the total number of PC units while I(B$_1$) and I(A$_2$) are the integral values of protons **B$_1$** and **A$_2$** representing the end groups. The value of repeating units allows to calculate $\overline{M_n}$ = 8500 g/mol^{-1}.

After polymerization of the ε-caprolactone, the characteristic peaks of the derived repetitive units are also observable (Figure 4.5). The signals at 1.38, 2.31 and 4.06 ppm are referred respectively to the protons: **F**, **D** and **H** of poly(ε-caprolactone) chain. Signals corresponding to the protons **E** and **G** of the same segment are overlapped in the spectrum at 1.65 ppm with the poly(carbonate) protons **C**. The signal at 2.56 ppm is assigned to protons **D** of the chain end confirming the formation of PC-PCL units, otherwise the signal would have been shifted at 2.31 ppm as previously reported.
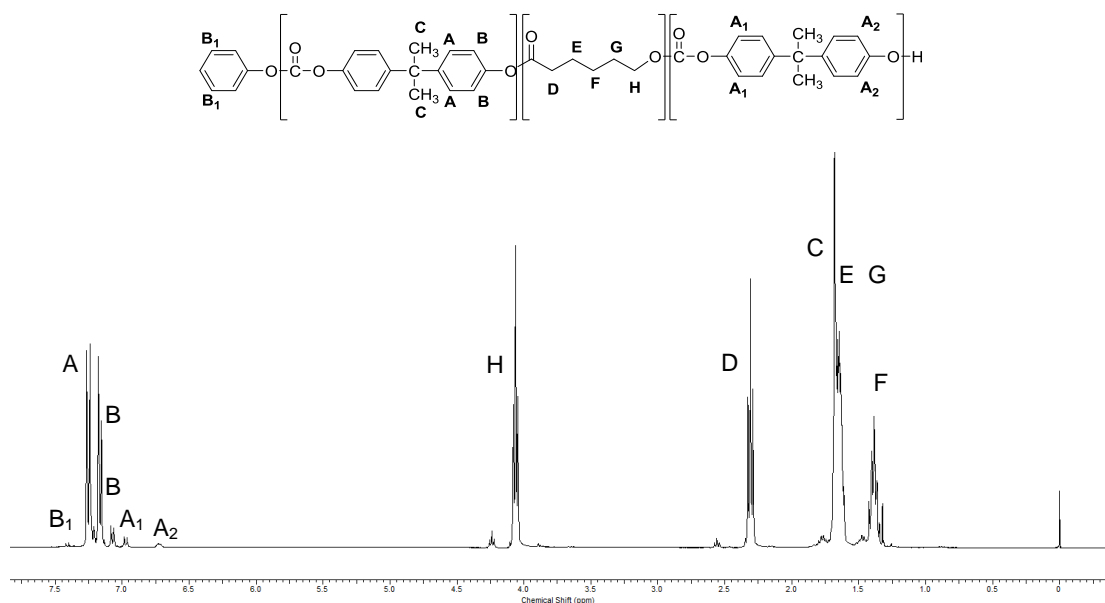
Figure 4.5: ¹H-NMR spectrum of the copolymer of poly(ε-caprolactone) and poly(carbonate) (PCL-*co*-PC).

As mentioned above, the signals at 7.25, 7.17 and 1.68 ppm are referred respectively to protons **A**, **B** and **C** present in the chain of poly(carbonate). The doublet at 7.07 ppm is assignable to the **B** protons of the chain end according to the chemical shift of the equivalent proton in a phenyl ester end-group of a PCL chain.

The signal at 4.24 ppm is assigned to protons **H** of the chain end of poly(ε-caprolactone). The doublet at 6.97 ppm is referred to protons **A₁** proving that transesterification reaction occurs. The signal at 6.70 ppm is assigned to protons **A₂** while the peak at 7.40 ppm is assigned to protons **B₁** of the poly(carbonate) phenylic end groups.

It is worth noting that the integral value of the peak at 7.07 ppm is equivalent to the sum of the integrals at 7.40, 6.97 and 6.70 ppm (Figure 4.5) suggesting that in each chain the protons **B** of the end-chain of poly(carbonate) are present. On the other hand, the poly(carbonate) chain can ends with protons **A₁**, **A₂** or **B₁** which are the protons of a phenyl carbonate end group of a PCL chain, of a phenolic end group and of a phenyl carbonate end group respectively.
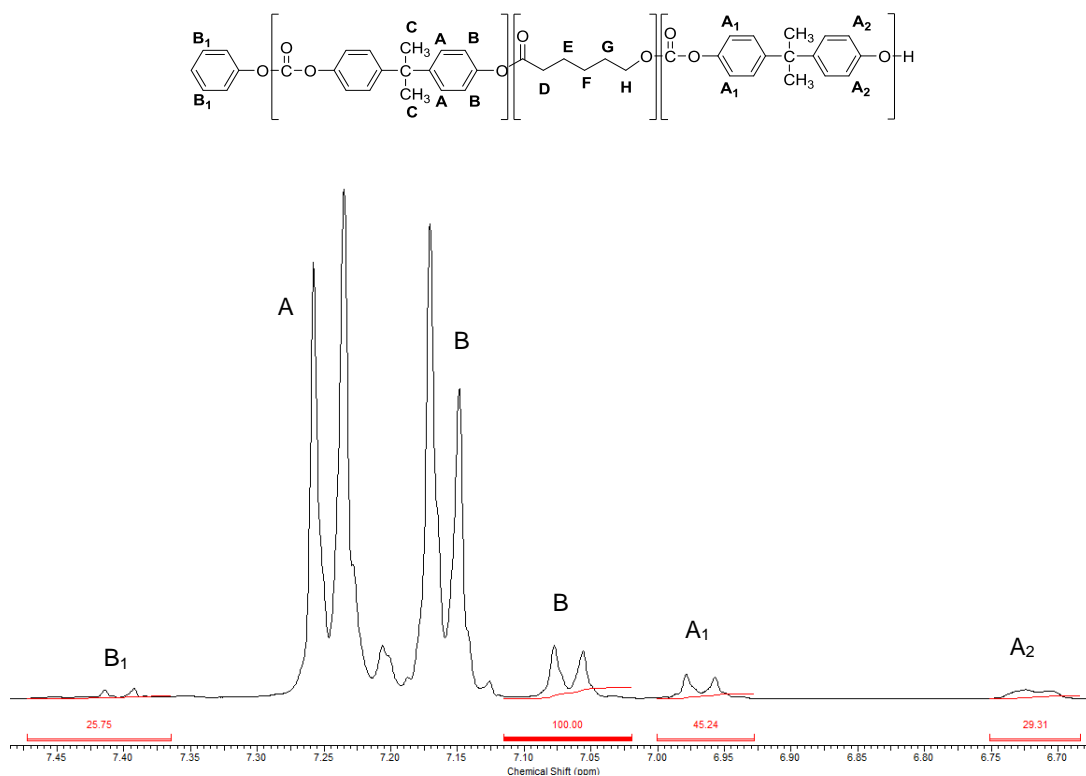
Figure 4.6: ^{1}H-NMR spectrum of the copolymer of poly(ε-caprolactone) and poly(carbonate) (PCL-*co*-PC).

From integration of ^{1}H-NMR signals, molar composition and relative quantities of different sequences are calculated.

The molar composition is calculated by integration of poly(carbonate) aromatic protons from 7.40 to 6.70 ppm and aliphatic protons of poly(ε-caprolactone) from 2.31 to 2.56 ppm. The following formula has been used:

$$\text{mol comp\%} = \frac{I(D)/2}{(I(D)/2) + ((\,I(A) + I(B) + I(A_1) + I(A_2) + I(B_1))/8)} \times 100 \quad \text{Eq. 4.2}$$

where I(D) is the integral value of protons **D** representing the aliphatic protons of poly(ε-caprolactone) while the other integral values shown in the equation represent the aromatic protons of poly(carbonate).

The length of poly(carbonate) block is calculated by the ratio of integrals at 7.16 ppm and at 7.07 ppm as shown in Equation 3. The first one is referred to protons **B** of the main chain while the second one to the same protons of end-groups.

$$PC \ unit = \frac{I(B_{main \ chain})/4}{I(B_{end \ chain})/2}$$

Eq. 4.3

On the other hand, the length of poly(ε-caprolactone) block is calculated by the ratio of integrals at 2.31 ppm and at 2.56 ppm referred to protons **D** of the main chain and of the end-group respectively.

$$PCL \ unit = \frac{I(D_{main \ chain})}{I(D_{end \ chain})}$$

Eq. 4.4

The conversion of the ε-caprolactone is calculated by integration of the signals at 2.64 and 2.31 referred to the protons **D** of the monomer and the polymer respectively in the reaction crude (Figure 4.7). The following formula has been used:

$$Conv. \ CL \ \% = \frac{I(D_{polymer})}{I(D_{polymer})+I(D_{monomer})} \times 100$$
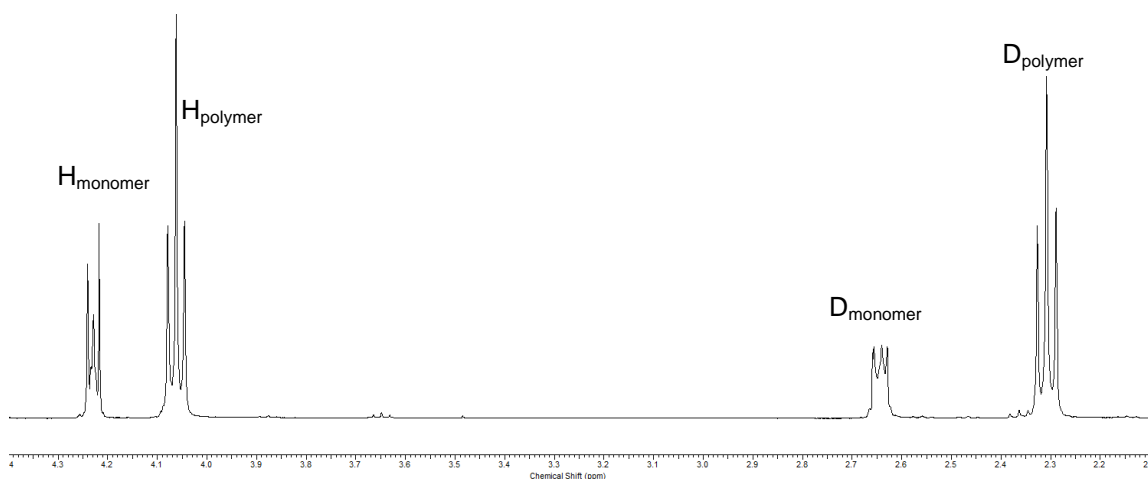
Eq. 4.5

Figure 4.7: ^{1}H-NMR spectrum of reaction crude.

By this method, the relative length of each PC and PCL sequences and the composition of the copolymers was calculated (Table 4.3). In the table it is also reported the molecular weight of each copolymer, obtained by GPC analysis.

Table 4.3: Molecular characteristics of copolymers. Composition (PCL w/w%), PC-PCL units length, average molecular weights ($\overline{M_w}$), and polydispersity (D).

Sample	Comp. PCL (w/w%)	PC length	PCL length	$\overline{M_w}$ (Da)	D
PCL-*b*-PC	49	3	35	18500	1.4
PCL-*ran*-PC	61	1	10	14600	2.3

4.2.2. Thermal characterization

The thermal behaviour of the synthetized copolymers has been investigated by non-isothermal DSC and TGA experiments.

The structure of the copolymers microdomains in the melt state depends on their segregation strength given by χN (where χ is the Flory–Huggins interaction parameter between different blocks and N the overall degree of polymerization of the entire block copolymer).[47] When χN is lower than 10, a single-phase melt is usually formed. On the other hand, when χN is higher than 10, copolymers segregate in two phases in the melt state.

As Table 4.4 shows, for each copolymer a value lower than 10 is obtained. It is therefore assumable that the copolymers form a single phase system in the melt state.

However, considering that in the second heating curves (Figure 4.8b) PCL-*b*-PC presents at 44 °C a melting peak relative to PCL crystals formed during the previous cooling, it is possible to assume that, in this case, a segregation of the phases happens during the cooling from the melt state.

Table 4.4: Molecular characteristic of the copolymers. The Flory-Huggins enthalpic segmental interaction parameter χ; the overall degree of polymerization of the copolymer calculated by $\overline{M_n}/\overline{M_0}$ where $\overline{M_n}$ is the number average molecular weight of the entire copolymer and $\overline{M_0}$ is the molecular weight of the repeating unit (taking into account the molar composition of the copolymer); glass transition temperature (T_g), temperature of crystallization (T_c) and melting (T_m) and relative enthalpy values.

Sample	χ	N	χ N	T_g (°C)	T_c (°C)	ΔH_c (J/g)	T_m (°C)	ΔH_m (J/g)
PCL-*b*-PC	0.075	99.7	7.5	-36	22	0.8	44	1
PCL-*ran*-PC	0.075	124.4	8.8	-32	-	-	-	-

On the other hand, PCL-*ran*-PC does not show any evidence of crystallization of the PCL phase but it must be considered that in this case the relative PCL sequences are too short to be rearranged during crystallization (Table 4.3).[58]
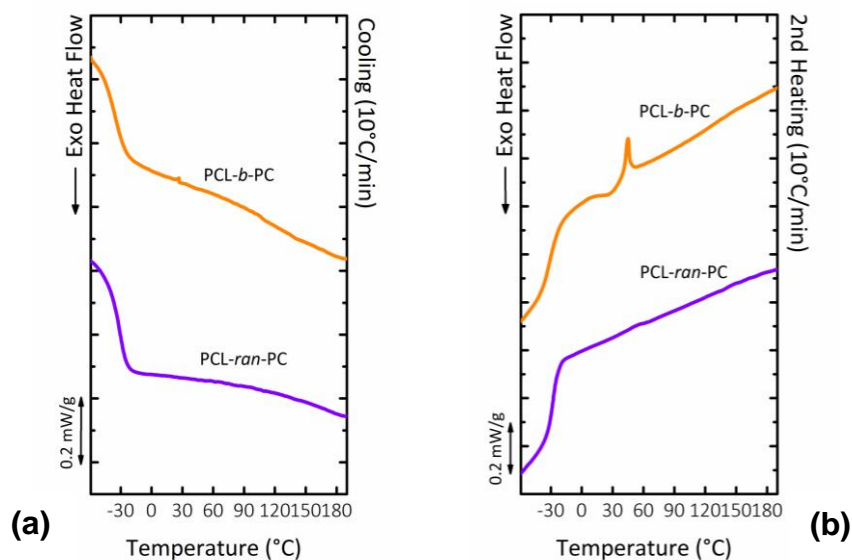
Figure 4.8: Non-isothermal DSC experiments on block and random copolymers. **(a)** cooling curves at 10 °C/min from the melt state; **(b)** subsequent heating curves at 10 °C/min. The curves have been normalized by the weight of the samples.

Figure 4.9 shows TGA results of PCL-*b*-PC and PCL-*ran*-PC copolymers and the respective derivative curves dw/dT as function of temperature, while in Table 4.5 are reported the respective values obtained from the curves.

Both copolymers present a single degradation step, as result of a single phase system formation in the melt state (χN is lower than 10 for both copolymers). However, the temperature at which PCL-*ran*-PC loses 10% of the total mass is 291 °C, whereas for PCL-*b*-PC it is 315 °C (Table 4.5).

Considering that the two copolymers have a similar composition, the different degradation behaviour is related to two factors. First of all, PCL-*b*-PC has a higher molecular weight than PCL-*ran*-PC, and thus the polymer chains need higher temperature to start degradation. At the same time, in PCL-*ran*-PC the number of linkages between different sequences (i.e., PC and PCL blocks) is higher than in PCL-*b*-PC. Being PCL-PC linkage more susceptible to degradation than PC-PC or PCL-PCL linkages, PCL-*ran*-PC starts its degradation before PCL-*b*-PC.
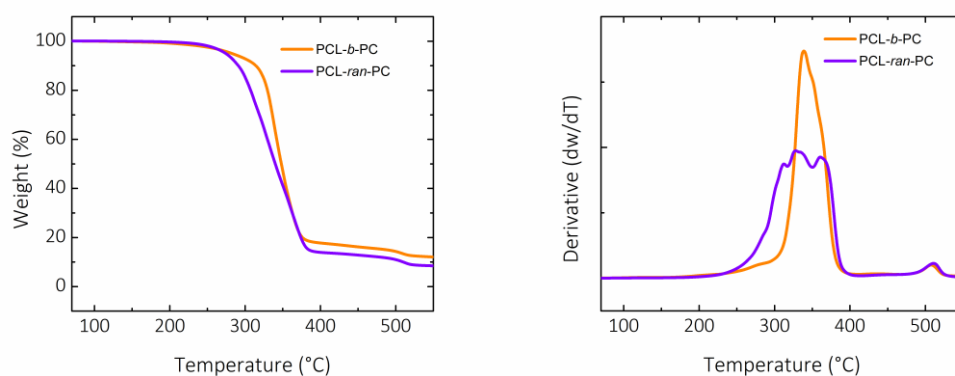
Figure 4.9: TGA curves of PCL-*b*-PC and PCL-*ran*-PC copolymers.

Table 4.5: Data obtained from TGA analysis for PCL-*b*-PC and PCL-*ran*-PC copolymers.

Sample	T 10% loss (°C)	T derivate peak (°C)
PCL-*b*-PC	315	339
PCL-*ran*-PC	291	329

4.3.   Characterization of PLA/PCL based blends

4.3.1. Preparation of the blends

A constant PLA/PCL weight ratio of 80/20 was employed in order to obtain a well-balanced combination of stiffness and toughness. PCL-PC based copolymers were tested as compatibilizers by adding them at 10% by weight with respect to the minor phase. Thus, the final blends have an approximate composition of 80/20/2, weight ratio, PLA/PCL/PCL-*co*-PC. The blends were prepared by both solution and melt mixing.

In the first case, neat homopolymers and the PCL-PC based copolymers were dissolved in dichloromethane and stirred at room temperature. The film forming solutions were casted until constant weight was reached.

In the second case, neat homopolymers and the PCL-PC based copolymers were melted and blended in a twin-screw extruder (screw speed: 200 rpm, temperature: 200°C, residence time: 1 minute). The extruded filaments were rapidly quenched in a water bath and pelletized.

The blends prepared by solution mixing have been designated with: (s) while the corresponding ones prepared by melt blending have been designated with: (m).

It is worth noting that upon the two different blending techniques, different morphologies and thermal behaviours of the resulting blends are obtained.

In melt mixing, samples are heated at a temperature higher than T_m and subjected to shear within the extruder. This process can cause a direct degradation of the polymer, which results in a shortening of the chains. On the other hand, in solution mixed samples, the blend components remain at room temperature in a hydrophobic solvent, which should prevent the chains degradation. Because molecular weight has a key role in determining most of the properties of the blend, each of the following results must be correlated to a possible change in the molecular weight.

It is also important to consider that the migration of heterogeneities from one phase to the other, which could change crystallization kinetics, in melt mixed blends happens directly from one phase to the other whereas in solution mixed blends it could happen from one phase to the solvent.

At the same time, upon solution or melt blending a different morphology of the blend can be obtained. On one hand, in solution mixed blends the size of the minor phase domains is mainly dependent on the respective interfacial tension between the phases during segregation upon solvent evaporation. On the other hand, in melt mixed sample, the size of the minor phase domains is also correlated with the balance between coalescence and breakup of the droplets and therefore to the processing parameters. Furthermore, as a general result, in solution mixed sample the size of the minor phase domains is typically higher than in melt mixed blend upon the mechanical dispersion of one phase in the other.

In the following paragraphs, results for both solution and melt mixed blends at the same respective compositions will be presented.

4.3.2. Molecular weight analysis

Table 4.6 reports average and numerical molecular weight of neat PLA and PLA phase within the blends, while in Figure 4.10 a schematic chart representative of the molecular weight variation upon blending is illustrated.

In all solution blended samples, the molecular weight does not change upon blending and it is assumable that PLA phase molecular weight is maintained

unchanged with respect to the nominal value reported by the producer (i.e., $\overline{M_w}$ = 180 KDa).

On the contrary in melt blended samples, the molecular weight is always lower than expected and it is even further influenced by copolymers addition. If on one hand, the molecular weight of neat PLA and PLA/PCL is only slightly decreased, on the other hand, copolymers addition causes a dramatic degradation of the polymers chains. In particular, in PLA/PCL/PCL-*b*-PC, the $\overline{M_w}$ value is decreased to 113 KDa while in PLA/PCL/PCL-*ran*-PC $\overline{M_w}$ is even decreased to 64 KDa. Considering that all melt blended samples have been processed in the same way, such reduction of the molecular weight must be induced by copolymer addition.

It is assumable that PCL-PC based copolymers, characterized by low molecular weights (Table 4.3), are more susceptible than PLA phase to degradation at melt blending conditions. Once degraded to polymers with lower molecular weight, they can undergo transesterification with PLA chains causing such molecular weight reductions.

As confirmation, it is worth noting that the copolymer characterized by the lowest molecular weight and thus the most susceptible to degradation (i.e., PCL-*ran*-PC, see molecular weight in Table 4.3 and thermograms in Figure 4.9) is the one that cause the highest molecular weight reduction.

In order to further confirm such hypothesis a thermogravimetric analysis was performed.

Table 4.6: Average molecular weight of melt blended and solvent mixed samples.

Sample	$\overline{M_n}$ (KDa)	$\overline{M_w}$ (KDa)	D
PLA(m)	123	153	1.2
PLA/PCL(m)	111	160	1.4
PLA/PCL/PCL-*b*-PC(m)	81	113	1.4
PLA/PCL/PCL-*ran*-PC(m)	38	64	1.7
PLA(s)	117	179	1.5
PLA/PCL(s)	116	178	1.5
PLA/PCL/PCL-*b*-PC(s)	132	179	1.4
PLA/PCL/PCL-*ran*-PC(s)	127	184	1.4
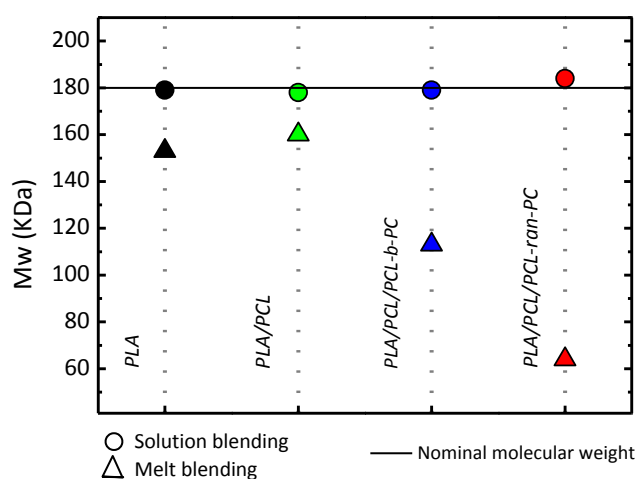
Figure 4.10: Schematic representation of molecular weight variation upon melt blending.

4.3.3. Thermogravimetric analysis

Figure 4.11 shows the thermograms and respective derivatives (dw/dT) of neat PLA, PLA/PCL and PLA/PCL/PCL-*co*-PC, for both the blends obtained by melt and solution mixing, while in Table 4.7 are reported the corresponding temperatures of 10% loss and derivative peak maximum.

Neat PLA starts its degradation at temperatures above 305 °C in agreement with the study of Carrasco *et al.*[59] and without important differences between solvent cast and melt mixed samples.

Also, the PLA phase within PLA/PCL blends is not affected by processing condition (i.e., solution or melt blending) since both blends have a similar molecular weight (see Table 4.6) and thus the degradation occurs in the same temperature range.

On the other hand, the degradation temperature of PLA/PCL/PCL-*co*-PC depends on the processing condition (as reflection of the differences in molecular weight, see Table 4.6). According to Table 4.7, PLA/PCL/PCL-*b*-PC(s) loses the 10% of the total mass at T=317 °C whereas PLA/PCL/PCL-*b*-PC(m) at T=280 °C. At the same time, PLA/PCL/PCL-*ran*-PC(s) loses the 10% of the total mass at T=310 °C whereas PLA/PCL/PCL-*ran*-PC(m) loses the 10% of the total mass at T=272 °C.
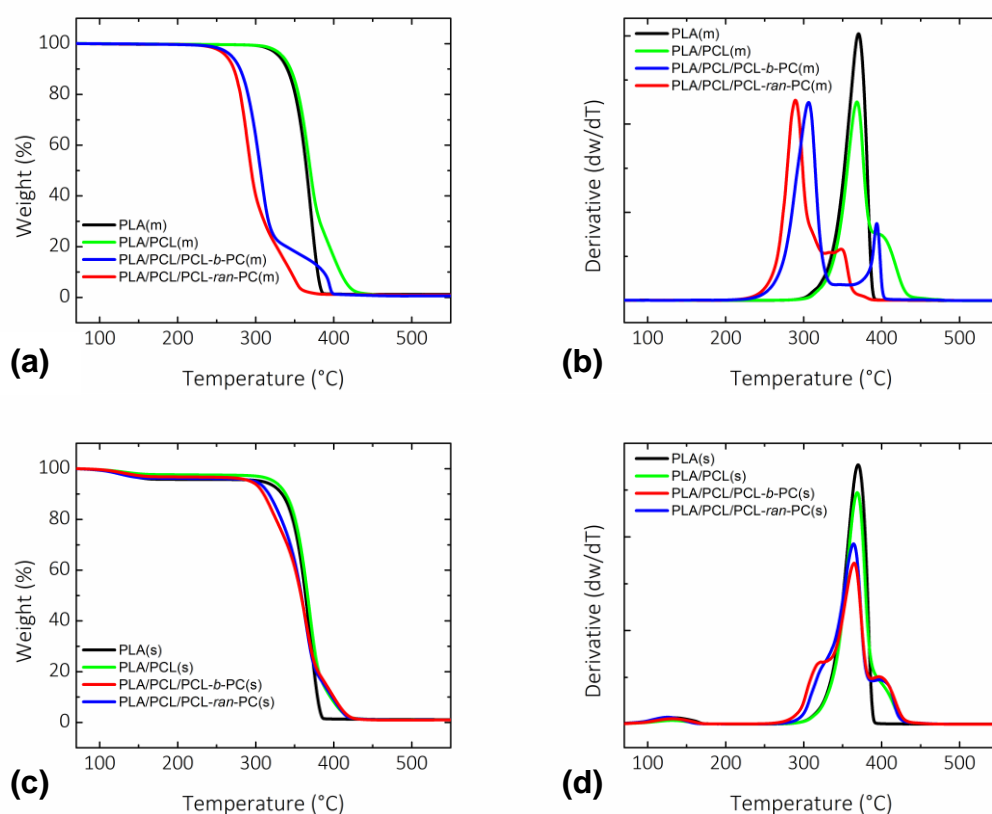
Figure 4.11: Thermograms of the blends. (a) Weight reduction of neat PLA and PLA/PCL, PLA/PCL/PCL-*co*-PC blends, obtained by melt blending; (b) Derivative curves (dw/dT) of neat PLA and PLA/PCL, PLA/PCL/PCL-*co*-PC blends, obtained by melt blending; (c) Weight reduction of neat PLA and PLA/PCL, PLA/PCL/PCL-*co*-PC blends, obtained by solution blending; (d) Derivative curves (dw/dT) of neat PLA and PLA/PCL, PLA/PCL/PCL-*co*-PC blends, obtained by solution blending.

Table 4.7: Data obtained for TGA analyses for neat PLA, PLA/PCL and PLA/PCL/PCL-*co*-PC blends. Blends obtained by both melt and solution mixing.

Sample	T 10% loss (°C)	T derivate peak (°C)
PLA(m)	340	370
PLA/PCL(m)	345	368
PLA/PCL/PCL-*b*-PC(m)	280	306
PLA/PCL/PCL-*ran*-PC(m)	272	290
PLA(s)	334	370
PLA/PCL(s)	339	369
PLA/PCL/PCL-*b*-PC(s)	317	364
PLA/PCL/PCL-*ran*-PC(s)	310	365

39

4.3.4. Morphological analysis

Figure 4.12 shows SEM micrographs of the cryogenically fractured surfaces of PLA/PCL and PLA/PCL/PCL-*co*-PC of the melt blended samples, while in Figure 4.13 are reported the micrographs of solution mixed samples.

Table 4.8 reports average PCL particles size within the blend measured by counting at least 100 particles for both the blends obtained by melt and solution. Number (d_n) and volume (d_v) average diameters and particle size polydispersity (D_p) were calculated by the following equations:

$$d_n = \frac{\sum_{i=1}^{n} n_i d_i}{\sum_{i=1}^{n} n_i} \qquad\qquad \text{Eq. 4.6}$$

$$d_v = \frac{\sum_{i=1}^{n} n_i d_i^4}{\sum_{i=1}^{n} n_i d_i^3} \qquad\qquad \text{Eq. 4.7}$$

$$D_p = \frac{d_v}{d_n} \qquad\qquad \text{Eq.4.8}$$

where n_i is the number of droplets 'i' of diameter d_i.

A *sea island* morphology, typical of immiscible blends, is observable in all cases. PLA conforms the matrix, while PCL is dispersed in droplets. The cavities observed in all the micrographs are due to the interfacial debonding between PLA and PCL during the fracture confirming the immiscibility between phases.

The differences in PCL particle size are strictly related to the blending technique. When two immiscible polymers are blended during melt mixing, one phase is mechanically dispersed inside the other. The size and shape of the minor phase particles depend on the establishment of equilibrium between drop breakup and coalescence.

On the other hand, in solution mixing the two polymer phases are not mechanically dispersed one inside the other, but rather are dissolved in a common solvent which provides to solubilize both the polymers. The absence of

a direct mechanical dispersion is reflected in general increase of the minor phase particles size and dispersion (D_p) as well.

According to Table 4.8, in all cases (both melt and solution mixed blends) the PCL particles size does not change upon copolymers addition. This indicates that the copolymers do not migrate to the PLA-PCL interphase, but, rather, are dispersed in one or both phases.

Table 4.8: Number average (d_n) and volume average (d_v) particle diameters, particle size distributions (D_p) and standard deviation (SD) of the PCL phase in PLA/PCL and PLA/PCL/PCL-*co*-PC blends. Blends obtained by both melt and solution mixing.

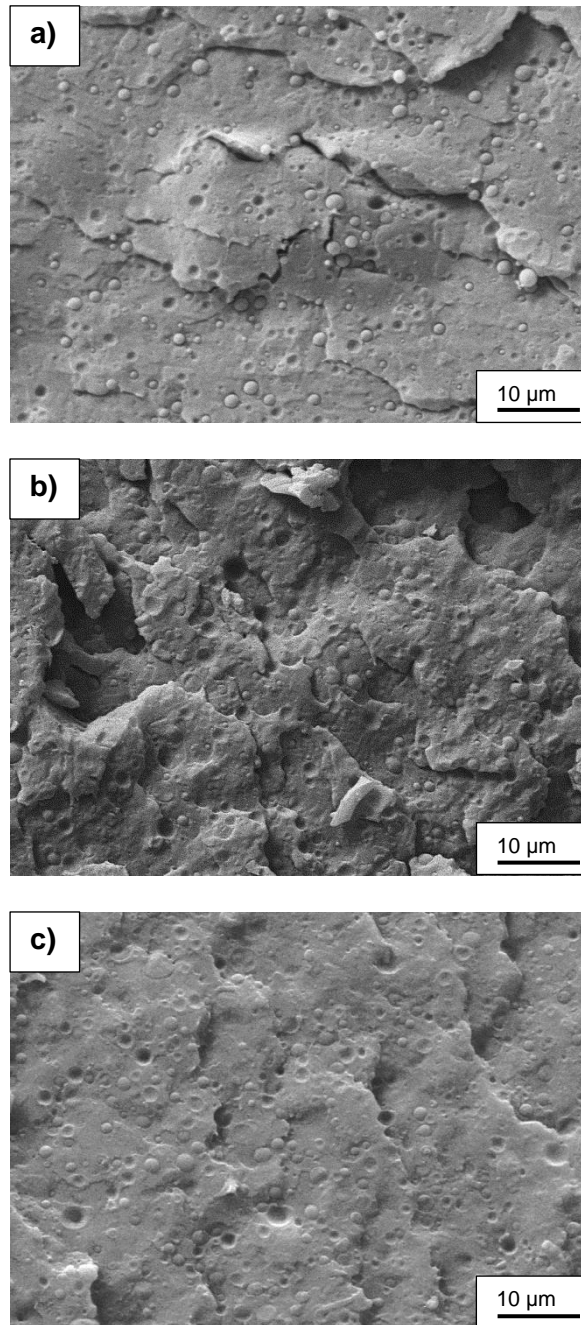| Sample	d_n (μm)	d_v (μm)	D_p	SD
PLA/PCL(m)	1.4	1.7	1.3	0.45
PLA/PCL/PCL-*b*-PC(m)	1.5	2.0	1.3	0.49
PLA/PCL/PCL-*ran*-PC(m)	1.7	2.3	1.4	0.52
PLA/PCL(s)	5.6	11.0	2.0	1.36
PLA/PCL/PCL-*b*-PC(s)	3.2	9.8	3.1	0.96
PLA/PCL/PCL-*ran*-PC(s)	6.2	13.2	2.1	2.48

Figure 4.12: SEM micrographs of the cryogenically fractured surfaces of (a) PLA/PCL(m), (b) PLA/PCL/PCL-*b*-PC(m), (c) PLA/PCL/PCL-*ran*-PC(m) blends obtained by melt mixing.
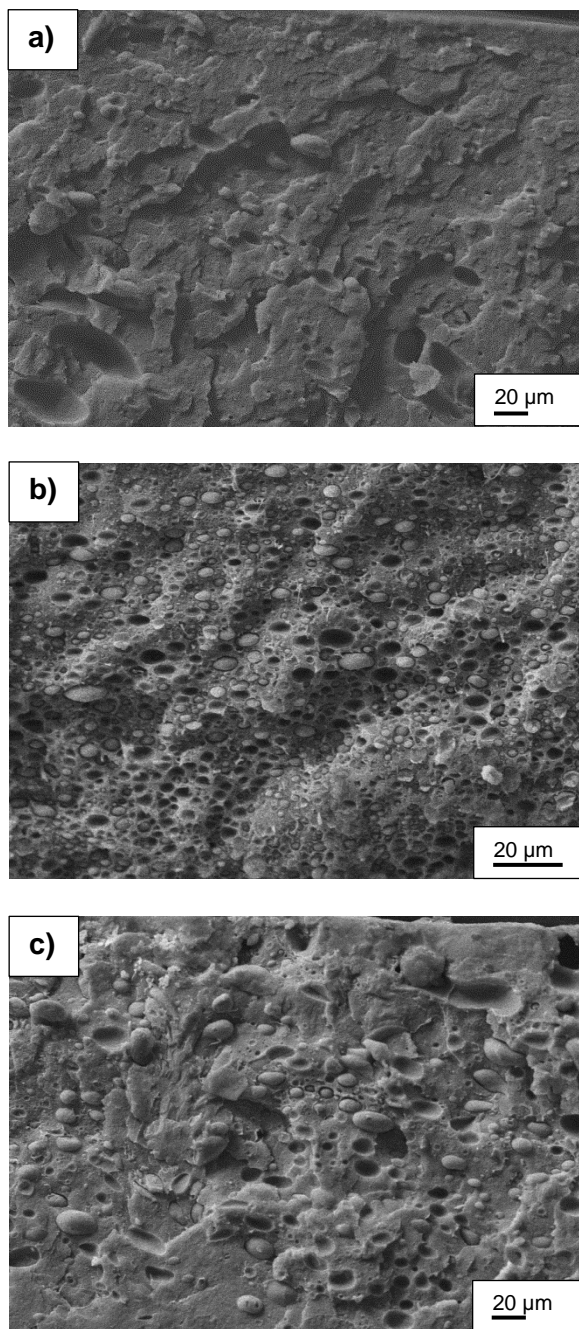
Figure 4.13: SEM micrographs of the cryogenically fractured surfaces of (a) PLA/PCL, (b) PLA/PCL/PCL-*b*-PC, (c) PLA/PCL/PCL-*ran*-PC blends obtained by solution mixing.

4.3.5. Non-isothermal DSC analysis - Cooling from the melt state

Figure 4.14 and Figure 4.15 show cooling DSC curves at 10 °C/min from the melt state for all the products: neat components, PLA/PCL and PLA/PCL/PCL-*co*-PC. While in Table 4.9 are reported the corresponding values of thermal transitions recorded during the scan.

In all the curves present in Figure 4.14 and Figure 4.15, the step recorded in the range between 59-61 °C corresponds to the glass-transition temperature T_g of PLA phase.

Upon blending with PCL, both in solution and melt mixing, T_g of PLA phase remains constant, proving that there is not an enhancement in miscibility between the PLA phase and the PCL one. Otherwise, a T_g depression would be detected, as result of the interaction of PLA with the more flexible PCL chains (PCL T_g = -60 °C).

It is worth noting that this result confirms the previous hypothesis, detected by morphological analysis of the blends, that copolymers do not migrate to the PLA-PCL interphase but, rather, are dissolved in one or both the phases.

Neat PCL crystallizes during cooling with a sharp exothermic peak, at 26 °C in the case of melted sample (PCL(m)) and at 29 °C in the case of solution mixed sample (PCL(s)). In the case of melt mixed PLA/PCL(m), PCL crystallization is fractionated into two peaks at 24 °C and 35 °C whereas in solution mixed PLA/PCL(s) the same occurrence does not happen.

The fractionation of the crystallization is a common occurrence in immiscible blends. It happens when the number of droplets of a crystallizable phase is larger or of the same order of magnitude as the number of active heterogeneities in the bulk polymer before being dispersed. The smaller the droplets, the more difficult would be to find active heterogeneities in each droplet.

In melt mixed PLA/PCL(m), the first crystallization peak at 35 °C corresponds to the crystallization of PCL droplets that have been nucleated by the same active heterogeneities present in the bulk polymer. The second crystallization peak at 24 °C regards the crystallization of PCL droplets nucleated by less active heterogeneities.[21,22]

On the other hand, in solution mixed PLA/PCL(s) the same occurrence does not happen since droplets size is larger than in the corresponding melt mixed blend and therefore only one peak at 33 °C is registered.

In the case of melt mixed blends containing PCL-PC based copolymers (i.e., PLA/PCL/PCL-*b*-PC(m) and PLA/PCL/PCL-*ran*-PC(m)) a single PCL crystallization peak at 36 °C is detected, even though the particle size is the same as the corresponding melt mixed PLA/PCL(m) blend (see Table 4.8). In this case, all PCL droplets crystallize at higher temperatures since the addition of the copolymers in the melt state probably causes a transfer of heterogeneities to the PCL phase.

Also in the case of solution mixed blends containing PCL-PC based copolymers (i.e., PLA/PCL/PCL-*b*-PC(s) and PLA/PCL/PCL-*ran*-PC(s) blends) a single PCL crystallization peak is detected. However, in this case, the temperature of crystallization is detected at 32 °C, a temperature quite lower than that in the corresponding blends obtained by melt blending (see Table 4.9). This is probably caused since during the dissolution process the active heterogeneities that activated PCL crystallization at higher temperature are dissolved in the solvent without migrating into PCL phase.

According to Figure 4.14 and Figure 4.15, neat PLA doesn't crystallize during cooling at the scanning rate employed, both in the sample obtained by solution and melt blending. This is because the amount of D-units in PLA (i.e., PLA 4032D 1.2-1.6% of D-unit)[23] is too high to allow chains alignments during crystallization at the employed scanning rates.

PLA is able to crystallize only in the melt mixed blends (no crystallization exotherms are detected in solution mixed samples). In particular, a dramatic PLA phase exotherm at 115 °C is detected in PLA/PCL/PCL-*ran*-PC(m), whereas a smaller exotherm is detected in the others blends.

Considering that no effect of increased miscibility between PLA and PCL phases are detected upon copolymers addition, the reason of this behaviour derives from the differences of processing condition between solution and melt mixing. In particular, it is assumable that the degradation of the melt mixing blends (see Table 4.6) is responsible of the increased PLA crystallinity, as a result of the increased chain mobility upon molecular weight reduction.

As confirmation, it is worth noting that the blend characterized by lowest molecular weight (i.e., PLA/PCL/PCL-*ran*-PC(m)) is the one that presents the greatest PLA crystallization enthalpy.

In any case, the crystallization of PLA phase within the blends, being the topic of this work, will be further analysed by isothermal analysis.

Figure 4.14: Non-isothermal DSC experiments curves. Cooling curves at 10 °C/min from the melt state of neat PLA, neat PCL, PLA/PCL and PLA/PCL/PCL-*co*-PC blends obtained by melt mixing. The curves have been normalized by the weight of the samples.
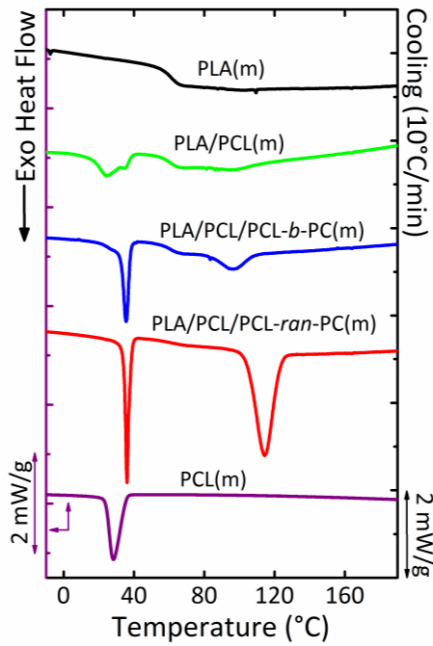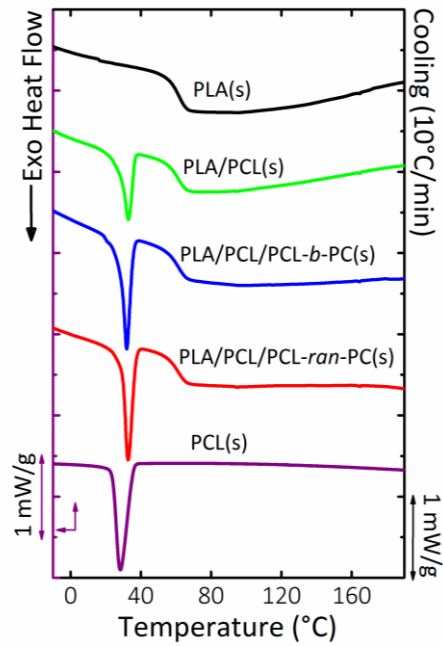
Figure 4.15: Non-isothermal DSC experiments curves. Cooling curves at 10 °C/min from the melt state of neat PLA, neat PCL, PLA/PCL and PLA/PCL/PCL-*co*-PC blends obtained by solution mixing. The curves have been normalized by the weight of the samples.

46

Table 4.9: Thermal properties obtained from non-isothermal DSC cooling at 10 °C/min. The enthalpies of crystallization and melting have been normalized by the weight fraction of the samples.

		Cooling				
		PCL		PLA		
Sample	Comp w/w	T_c (°C)	ΔH_c (J/g)	T_g (°C)	T_c (°C)	ΔH_c (J/g)
PLA(m)	100	-	-	59.6	-	-
PLA/PCL(m)	80/20	24.3/34.5	8.7/36.1	59.3	94.3	4.1
PLA/PCL/PCL-*b*-PC(m)	80/20/2	35.5	49.9	59.6	96.5	9.1
PLA/PCL/PCL-*ran*-PC(m)	80/20/2	36.0	56.8	61.9	114.5	42.0
PCL(m)	100	25.9	45.7	-	-	-
PLA(s)	100	-	-	59.6	-	-
PLA/PCL(s)	80/20	32.9	26	59.5	-	-
PLA/PCL/PCL-*b*-PC(s)	80/20/2	31.9	41.5	59.4	-	-
PLA/PCL/PCL-*ran*-PC(s)	80/20/2	32.7	43.2	59.7	-	-
PCL(s)	100	28.8	57.2	-	-	-

4.3.6. Non-isothermal DSC analysis - Second Heating

Figure 4.16 and Figure 4.17 show second heating DSC curves at 10 °C/min for neat components and all the blends, both obtained for melt and solution mixing. While in Table 4.10 the corresponding values obtained from the scans are reported.

Neat PLA undergoes to cold crystallization and the subsequent fusion of the produced crystals at respectively 115 °C and 167 °C for PLA(m), and 129 °C and 166 °C for PLA(s). In any case, the direct correspondence of enthalpy of crystallization and melting indicate that PLA remains completely amorphous during previous cooling in both the samples (see Table 4.10).

Upon blending with PCL, the cold crystallization exothermic peak is sharper and shifted to lower temperatures for both melt solution and melt mixed samples.

This occurs because PCL can nucleate PLA during aging below T_g.

This occurrence was already demonstrated in a previous work[14], where the decrease in T_{cc} of PLA upon blending with PCL in solution mixed sample was attributed to a nucleation effect of PCL on the glassy PLA matrix.

The melting temperature of PLA phase is maintained almost identical in all the samples, with the exception of PLA/PCL/PCL-*ran*-PC(m), where a double melting peak is detected, which could be a result of PLA polymorphism. As it is reported in the literature, depending on the conditions (i.e., crystallization

temperature), different crystalline structures can be obtained. Crystallization at temperatures above 120 °C, from melt or solution, results in the most common and stable PLA polymorph, the α-form crystals. At temperature below 120 °C, α-form can be replaced by pseudohexagonal α'-form. In this case the molecule segments have the same 10_3 helical chain conformation adopted in α-form but with higher conformational disorder and lower packing density. More recent studies demonstrate that the α'-form crystal is preferentially formed only at crystallization temperatures below 100 °C, while at crystallization temperature between 100 and 120 °C α'-form coexist with α-form.[29]

In PLA/PCL(m) and PLA/PCL/PCL-*b*-PC(m), PLA crystallizes at temperatures corresponding to α'-form crystal formation. However a small exotherm appears just before the single melting peak indicating a transformation of disordered α'-form to the ordered α-form crystals.

On the other hand, in PLA/PCL/PCL-*ran*-PC(m), PLA crystallizes at temperature of coexistence of the two crystals forms. Therefore a double melting peak appears during the scan. However, any polymorphic behaviour would need to be corroborated by Wide Angle X ray Diffraction studies, which are outside the scope of the present work.

In order to understand the following results, another clarification must be carried out. As Table 4.6 shows, the molecular weight of PLA phase within the samples is not the same. In melt mixed blends, and especially in PLA/PCL/PCL-*ran*-PC(m), a lower molecular weight was found and thus a lower PLA melting temperature could have been anticipated. However, no significant change in melting temperature has been detected.

However, it must be considered that a change in the molecular weight does not necessarily provide a change in the melting temperature. In fact, T_m increases until reaching an asymptotical dependence at $\overline{M_n}$ higher than 50 KDa.

Since in all the blends PLA has a high enough molecular weight T_m is not sensible to $\overline{M_n}$ variation.
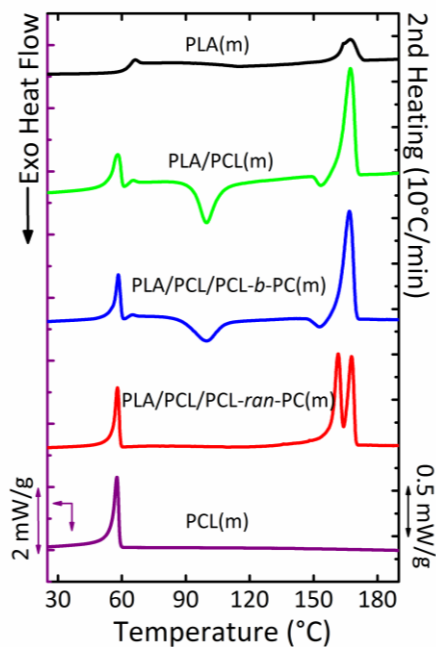
Figure 4.16: Non-isothermal DSC experiments. Second heating curves of neat PLA, neat PCL, PLA/PCL and PLA/PCL/PCL-*co*-PC blends obtained by melt mixing at 10 °C/min. The curves have been normalized by the weight of the samples.
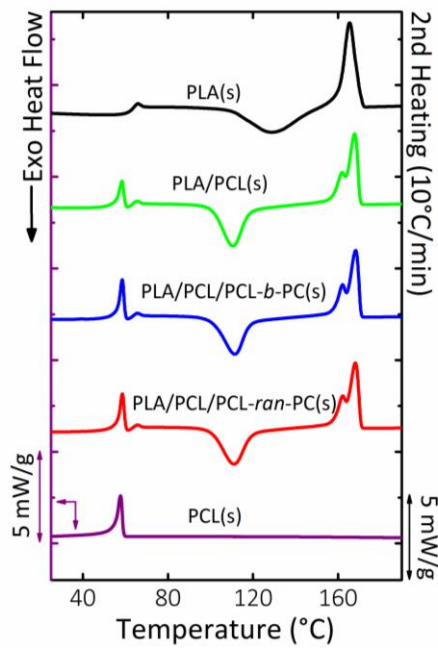
Figure 4.17: Non-isothermal DSC experiments. Second heating curves of neat PLA, neat PCL, PLA/PCL and PLA/PCL/PCL-*co*-PC blends prepared by solvent casting at 10 °C/min. The curves have been normalized by the weight of the samples.

Table 4.10: Thermal properties obtained from non-isothermal DSC heating at 10 °C/min. The enthalpies of crystallization and melting have been normalized by the weight fraction of the samples.

		Second Heating							
		PCL		PLA					
Sample	Comp w/w	T_m (°C)	ΔH_m (J/g)	T_{cc} (°C)	ΔH_{cc} (J/g)	T_{cc} (°C)	ΔH_{cc} (J/g)	T_m (°C)	ΔH_m (J/g)
PLA(m)	100	-	-	115.2	8.5	-	-	167.3	9.0
PLA/PCL(m)	80/20	58.0	40.1	99.8	25.6	153.6	2.9	167.3	36.9
PLA/PCL/PCL-*b*-PC(m)	80/20/2	58.4	42.2	99.7	21.4	152.9	2.8	166.8	39.0
PLA/PCL/PCL-*ran*-PC(m)	80/20/2	57.9	54.4	117.4	3.3	-	-	161.6/ 167.9	27.3/ 19.5
PCL(m)	100	55.3	46.6	-	-	-	-	-	-
PLA(s)	100	-	-	128.7	34.0	-	-	165.5	34.0
PLA/PCL(s)	80/20	58.4	30.0	110.5	35.8	-	-	161.8/ 167.8	14.3/ 23.5
PLA/PCL/PCL-*b*-PC(s)	80/20/2	58.4	40.7	111.3	31.5	-	-	162.3/ 168.3	12.1/ 21.7
PLA/PCL/PCL-*ran*-PC(s)	80/20/2	58.6	42.9	111.0	32.3	-	-	162.1/ 168.2	12.7/ 21.4
PCL(s)	100	57.8	63.2	-	-	-	-	-	-

4.3.7. Spherulitic growth kinetics of PLA phase

Figure 4.18 shows PLOM micrographs of neat PLA and PLA samples obtained by melt blending, while in Figure 4.19 the micrographs of the corresponding samples obtained by solution mixing are shown.

In all cases the spherulites show the typical Maltese cross morphology with a negative sign. However, upon blending spherulites get to be more fuzzy with a rougher morphology, furthermore some PCL droplets are evident inside the spherulites indicating that, although the two polymers are immiscible, a certain degree of compatibility is achieved during blending.
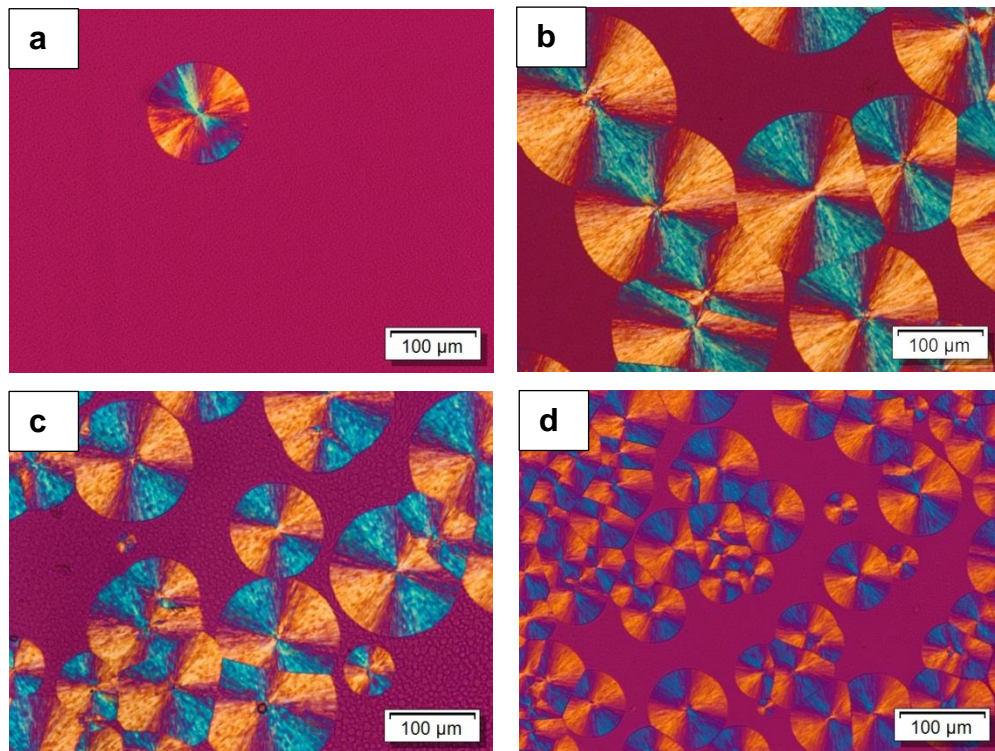

Figure 4.18: PLOM micrographs of (a) PLA(m) (b) PLA/PCL(m) (c) PLA/PCL/PCL-*b*-PC(m) (d) PLA/PCL/PCL-*ran*-PC(m) recorded at 130 °C and after 25 minutes from the beginning of crystallization.
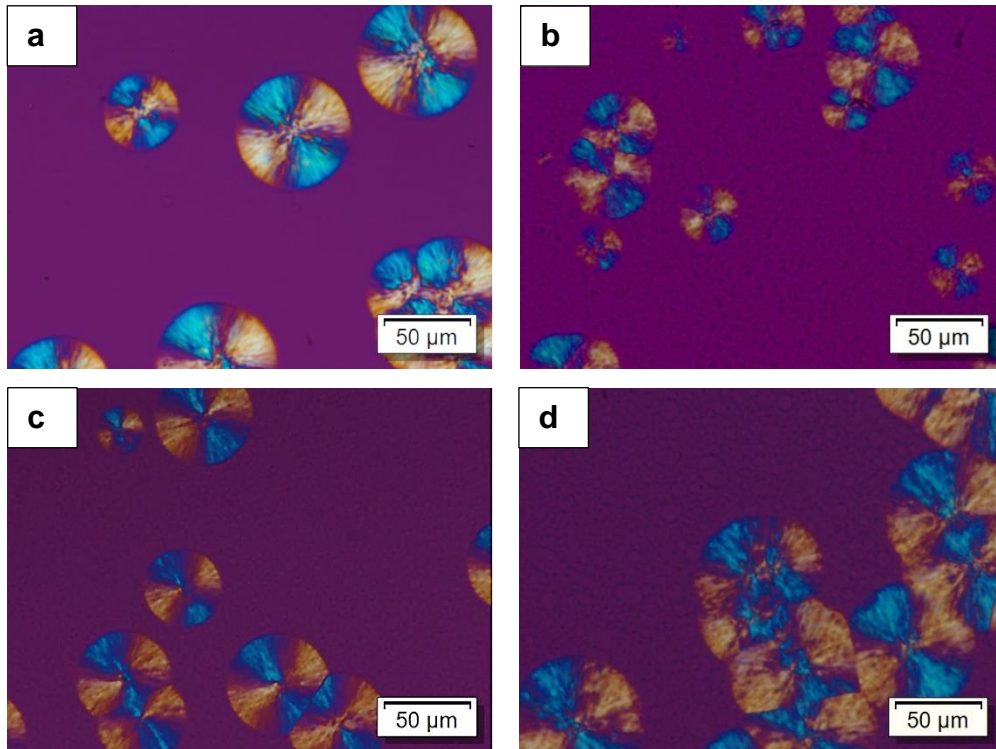
Figure 4.19: PLOM micrographs of (a) PLA(s) (b) PLA/PCL(s) (c) PLA/PCL/PCL-*b*-PC(s) (d) PLA/PCL/PCL-*ran*-PC(s) recorded at 130 °C and after 25 minutes from the beginning of crystallization.

In all samples, PLA spherulites grow linearly with time, indicating that no diffusion problems at the growth front were induced by blending. The spherulitic growth rate G (μm min^{-1}) was thus calculated from the slope of the line obtained from the spherulitic radius (μm) against time (min). The values of G at different crystallization temperatures were fitted by an arbitrary function to guide the eye.

All the sample show the well know behaviour of G as a function of T_c. Decreasing the temperature from T_m, the growth rate increases as result of the increased thermodynamic driving force for secondary nucleation. After it passes thought a maximum G decreases, upon the reduction of chain mobility with temperature.

Comparing Figure 4.20 with Figure 4.21, it is possible to see that for PLA/PCL/PCL-*b*-PC(m) and PLA/PCL/PCL-*ran*-PC(m) blends, G reaches values much larger than for neat PLA (in the case of PLA/PCL/PCL-*ran*-PC(m) a threefold increase of G is even detected). On the other hand, in the

51

corresponding solution mixed sample (i.e., PLA/PCL/PCL-*b*-PC(s) and PLA/PCL/PCL-*ran*-PC(s)) the values of G are almost the same of neat PLA. Considering that in none of the blends (both in melt and solution mixed samples as well) any evidence of increased miscibility between PLA and PCL phases is detected, the differences of growth kinetics must be due to the different molecular weights of PLA chains within the samples.

As it is well known, in a semicrystalline polymer the isothermal spherulitic growth rate decreases with molecular weight increase, as expected from the more restricted chain mobility, whereas it reaches a constant value for high enough molecular weights ($\overline{M_n}$ > 100 KDa).

As reported in Table 4.6, PLA/PCL/PCL-*b*-PC(m) and PLA/PCL/PCL-*ran*-PC(m), have a lower molecular weight than the other blends, because of the increased degradation of the chains (i.e., 38 KDa and 81 KDa in comparison with the other blends where $\overline{M_n}$ is always among 130 KDa). As a result in PLA/PCL/PCL-*b*-PC(m) and PLA/PCL/PCL-*ran*-PC(m) the spherulitic growth rate is higher.

Figure 4.20: Spherulitic growth rate G as a function of isothermal crystallization temperature T_c for neat PLA and PLA phase within PLA/PCL and PLA/PCL/PCL-*co*-PC melt mixed blends. The solid lines represent an arbitrary fit to guide the eye.
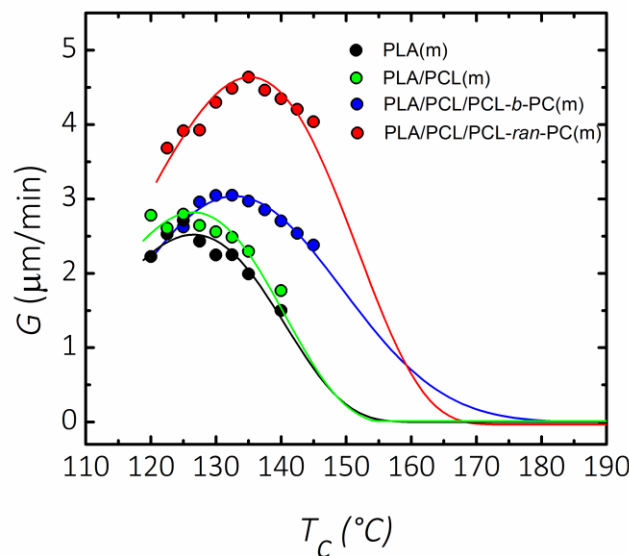
Figure 4.21: Spherulitic growth rate G as a function of isothermal crystallization temperature T_c for neat PLA and PLA phase within PLA/PCL and PLA/PCL/PCL-*co*-PC solvent mixed blends. The solid line represents an arbitrary fit to guide the eye.

4.3.8. Isothermal overall crystallization of PLA phase

The inverse of the half-crystallization time, determined by isothermal crystallization from the melt employing DSC, provides an experimental measure of the overall crystallization rate, which includes both nucleation and spherulitic growth.

Figure 4.22 shows plots of the overall crystallization rate (expressed as the inverse of half-crystallization time) as a function of temperature for melt blended samples, while in Figure 4.23 the plots are reported for the corresponding solution mixed samples.

The solid lines correspond to arbitrary fits performed to guide the eye. All the samples display the typical bell-shape trend, where the crystallization rate goes through a maximum as the kinetic changes from nucleation control at higher temperatures to diffusion control at lower temperatures.

Crystallization rate of neat PLA does not change upon different processing conditions. Both neat PLA samples, obtained by solution (Figure 4.22) and melt (Figure 4.23) processing as well, achieve their maximum relative crystallinity in 16 minutes at T_c=104 °C where the overall crystallization rate goes through a maximum. This result is consistent with the non-isothermal DSC cooling

53

experiments, in which no crystallization of PLA was detected during cooling, for both melt (Figure 4.14) and solution (Figure 4.15) processing samples.

At the same time, the effect of PCL blending to PLA phase crystallization rate is very similar for both melt and solution mixed sample. PLA/PCL(m) blend shows its maximum crystallization rate at T_c=108 °C and completes its crystallization after 10.8 minutes (Figure 4.22), while PLA/PCL(s) achieves its maximum relative crystallinity after 12 minutes at the same temperature (Figure 4.23).

Instead, upon the addition of PC-PCL based copolymers, the crystallization rate of PLA phase changes following the different processing condition (i.e., melt (Figure 4.22) or solution (Figure 4.23) blending).

As Figure 4.22 reports, PC-PCL based copolymers addition to melt mixed blends causes an enhancement of the crystallization rate. Taking neat PLA(m) as reference material, PLA/PCL/PCL-*b*-PC(m) shows a threefold increase, while in PLA/PCL/PCL-*ran*-PC(m) the crystallization rate is even ten times enhanced.

On the hand, PC-PCL based copolymers addition to solution mixed samples causes only slightly change to PLA crystallization rate. Taking neat PLA(s) as reference material, both PLA/PCL/PCL-*b*-PC(s) and PLA/PCL/PCL-*ran*-PC(s) complete their crystallization after respectively 11.2 and 16 minutes, values quite similar to neat PLA(s).

As it was already detected, the differences of crystallization kinetics must be due to the different molecular weights of PLA chains and mainly reflects the behaviour detected by isothermal spherulitic growth rate.

Figure 4.22: Isothermal crystallization experiments conducted after quenching the samples from the melt state. Overall crystallization rate ($1/t_{50\%}$) as a function of isothermal crystallization temperature T_c in neat PLA and PLA phase within PLA/PCL and PLA/PCL/PCL-*co*-PC melt mixed blends. The solid lines represent arbitrary fits to guide the eye.
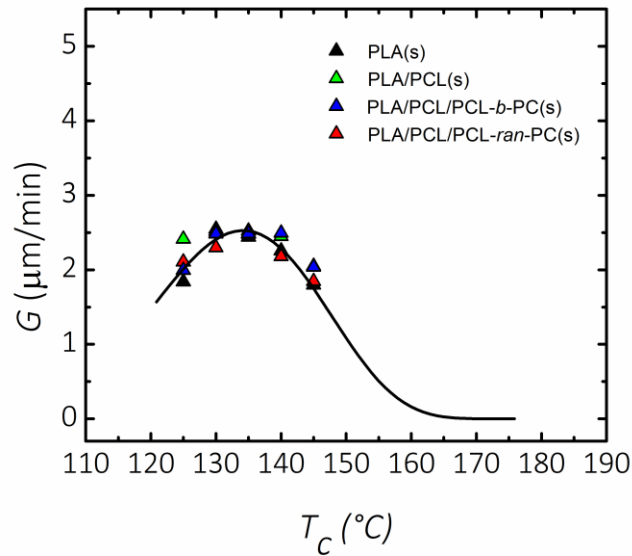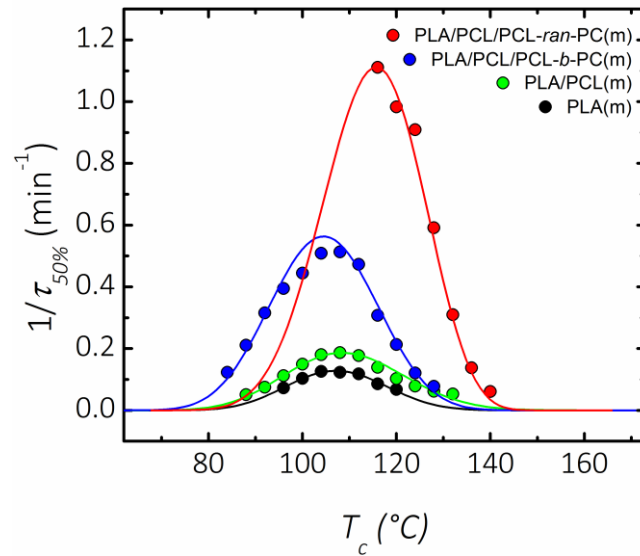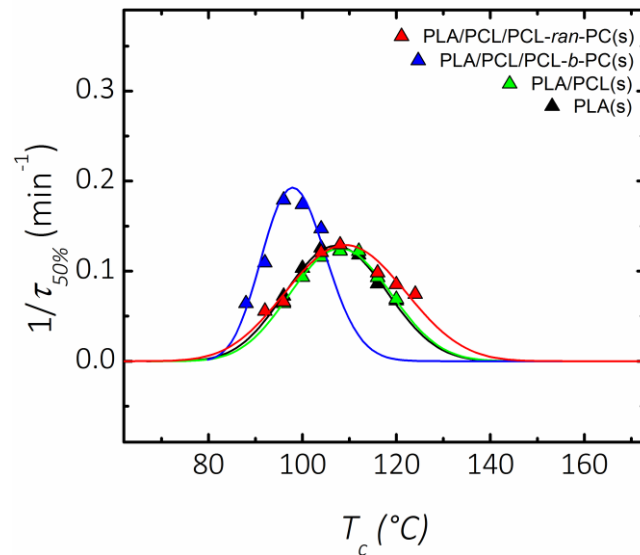

Figure 4.23: Isothermal crystallization experiments conducted after quenching the samples from the melt state. Overall crystallization rate ($1/t_{50\%}$) as a function of isothermal crystallization temperature T_c in neat PLA and PLA phase within PLA/PCL and PLA/PCL/PCL-*co*-PC solution mixed blends. The solid lines represent arbitrary fits to guide the eye.

The data obtained by isothermal DSC tests were used to develop the Avrami Fits and the graphical comparison between the experimental data and the prediction of the theory.

Firstly, in order to calculate the integral value of the isothermal DSC curve, the baseline has to be established. Secondly, the linear fit according to the Avrami equation can be performed.

The relative volume fraction crystallinity V_c is calculated according to Eq. 9 by setting 0.03 and 0.20 as range in order to obtain the best fit within the primary crystallization range.

$$V_c = \frac{W_c}{W_c + \frac{\rho_c}{\rho_a}(1-W_c)} \qquad \text{Eq. 4.9}$$

Where ρ_c and ρ_a are the densities of fully crystalline and fully amorphous polymer. For all calculation, the values of ρ_c = 1.359 g/cm3 and ρ_a = 1.25 g/cm3 were used for PLLA.

W_c that is the relative crystalline mass fraction is calculated by Eq. 10:

$$W_c = \frac{\Delta H_{(t)}}{\Delta H_{TOT}} \qquad \text{Eq. 4.10}$$

Where $\Delta H_{(t)}$ is the enthalpy value as a function of crystallization time and ΔH_{TOT} is the enthalpy value after completion of the crystallization process.

Finally, the Avrami equation is rearranged as follows:

$$\log[-\ln(1-V_c)] = \log(k) + n\log(t-t_0) \qquad \text{Eq. 4.11}$$

Where n is the Avrami index and k is the overall crystallization rate constant. The experimental and predicted half-crystallization $t_{50\%}$ is determined by an Origin® plugin developed by Lorenzo et al.[25]

According to the Avrami equation, $t_{50\%}$ is calculated by the following equation:

$$t_{50\%} = \left[-\frac{\ln[1-V_c]}{k}\right]^{1/n} \qquad \text{Eq. 4.12}$$

It is worth noting that depending on the goodness of the fit there may be a difference between the experimental and predicted values of $t_{50\%}$. The parameters obtained by Avrami Fits are collected in Table 4.11 and Table 4.12.

The Avrami index value (n) may range between 1 and 4 and it's the result of two contributions: the dimensionality of the crystals formed during crystallization (3D, 2D or 1D) and the nucleation time dependence (whose limits are sporadic and instantaneous). Crystals formed during crystallization could have one, two or three dimension producing a contribution of 1, 2 or 3 respectively in the n value. On the other hand, the nucleation could be instantaneous or sporadic. The instantaneous nucleation gives a contribution equal to 0 while the sporadic one equal to 1. By the sum of these two contributions the Avrami index value n is calculated.

Neat PLA and PLA phase within the blends, show most cases values not higher than 3. Considering that in all the blends 3D dimensional crystals are detected (spherulites), PLA nucleates mostly instantaneously.

Table 4.11: Data obtained by the Avrami model for melt mixed blends.

T_c	$t_{50\% theo}$ (min)	$t_{50\% exp}$ (min)	n	K (min^{-n})	R^2	$1/t_{50\% exp}$ (min^{-1})
PLA(m)						
120	16.645	16.317	3.03	1.40E-04	0.9995	0.0535
116	15.195	14.866	2.97	2.12E-04	1.0000	0.0580
112	9.567	8.467	2.70	5.81E-03	0.9988	0.1181
108	9.015	8.117	2.18	5.74E-03	0.9989	0.1232
104	8.572	7.950	2.31	4.89E-03	0.9994	0.1258
100	10.295	9.684	2.43	2.42E-03	0.9996	0.1033
96	14.922	13.817	2.43	9.85E-04	0.9993	0.0724

T_c	$t_{50\% theo}$ (min)	$t_{50\% exp}$ (min)	n	K (min^{-n})	R^2	$1/t_{50\% exp}$ (min^{-1})
PLA/PCL(m)						
128	16.979	16.300	2.62	4.10E-04	0.9999	0.0613
124	13.135	12.816	2.68	6.98E-04	0.9999	0.0780
120	9.788	9.750	2.72	1.41E-03	1.0000	0.1026
116	7.325	7.184	2.59	3.98E-03	0.9999	0.1392
112	5.711	5.634	2.69	6.36E-03	1.0000	0.1775
108	5.200	5.366	3.18	3.69E-03	0.9997	0.1864
104	5.415	5.550	3.14	3.44E-03	0.9998	0.1802
100	6.604	6.700	3.03	2.28E-03	1.0000	0.1493
96	8.972	8.917	3.00	9.65E-04	0.9999	0.1121
92	13.862	13.367	2.87	3.63E-04	0.9993	0.0748

T_c	$t_{50\% theo}$ (min)	$t_{50\% exp}$ (min)	n	K (min^{-n})	R^2	$1/t_{50\% exp}$ (min^{-1})
PLA/PCL/PCL-*b*-PC(m)						
128	14.162	12.833	2.39	1.23E-03	0.9983	0.0779
124	8.402	8.300	3.34	5.71E-04	0.9999	0.1205
120	4.767	4.700	3.48	3.01E-03	0.9996	0.2128
116	3.202	3.250	3.89	7.48E-03	1.0000	0.3077
112	2.054	2.116	3.97	3.99E-02	0.9998	0.4726
108	1.882	1.950	4.00	5.53E-02	1.0000	0.5128
104	1.905	1.966	4.19	4.66E-02	1.0000	0.5086
100	2.18	2.250	4.58	1.95E-02	1.0000	0.4444
96	2.513	2.533	4.02	1.71E-02	0.9998	0.3948
92	3.152	3.166	3.96	7.34E-03	0.9997	0.3159
88	4.725	4.750	3.89	1.64E-03	0.9997	0.2105
84	8.091	8.133	3.83	2.31E-04	0.9998	0.1230

	PLA/PCL/PCL-*ran*-PC(m)					
T_c	$t_{50\% \text{ theo}}$ (min)	$t_{50\% \text{ exp}}$ (min)	n	K (min^{-n})	R^2	$1/ t_{50\% \text{ exp}}$ (min^{-1})
140	17.707	16.450	2.69	3.00E-04	0.9991	0.0608
136	7.195	7.266	3.18	1.30E-03	1.0000	0.1376
132	3.118	3.233	3.33	1.58E-02	0.9999	0.3093
128	1.750	1.691	3.05	1.39E-01	0.9999	0.5914
124	1.072	1.100	3.31	5.51E-01	0.9999	0.9091
120	0.989	1.017	3.02	7.16E-01	1.0000	0.9833
116	0.894	0.900	2.85	9.53E-01	1.0000	1.1111

Table 4.12: Data obtained by the Avrami model for solvent mixed blends.

	PLA(s)					
T_c	$t_{50\% \text{ theo}}$ (min)	$t_{50\% \text{ exp}}$ (min)	n	K (min^{-n})	R^2	$1/t_{50\% \text{ exp}}$ (min^{-1})
120	14.814	14.916	2.27	1.52E-03	0.9997	0.0670
116	12.742	11.634	2.09	3.40E-03	0.9999	0.0860
112	9.567	8.467	2.12	5.81E-03	0.9988	0.1181
108	9.015	8.117	2.18	5.74E-03	0.9989	0.1232
104	8.572	7.950	2.31	4.89E-03	0.9994	0.1258
100	10.295	9.684	2.43	2.42E-03	0.9996	0.1033
96	14.922	13.817	2.43	9.85E-04	0.9993	0.0724

	PLA/PCL(s)					
T_c	$t_{50\% \text{ theo}}$ (min)	$t_{50\% \text{ exp}}$ (min)	n	K (min^{-n})	R^2	$1/t_{50\% \text{ exp}}$ (min^{-1})
120	14.731	14.533	2.15	2.14E-03	0.9992	0.0688
116	12.389	10.750	1.95	5.14E-03	0.9991	0.0930
112	9.606	8.184	2.17	5.09E-03	0.9956	0.1222
108	8.818	8.167	2.36	4.05E-03	0.9991	0.1224
104	9.317	8.650	2.35	3.65E-03	0.9989	0.1156
100	11.432	10.734	2.52	1.50E-03	0.9991	0.0932
96	15.156	15.584	3.74	2.66E-03	0.9996	0.0642

	PLA/PCL/PCL-*b*-PC(s)					
T_c	$t_{50\% \text{ theo}}$ (min)	$t_{50\% \text{ exp}}$ (min)	n	K (min^{-n})	R^2	$1/t_{50\% \text{ exp}}$ (min^{-1})
104	7.487	6.800	2.46	4.92E-03	0.9994	0.1471
100	5.999	5.750	3.18	2.33E-03	0.9997	0.1739
96	5.539	5.584	3.23	2.77E-03	1.0000	0.1791
92	8.718	9.150	3.64	2.61E-04	0.9998	0.1093
88	14.594	15.600	4.2	8.97E-06	0.9992	0.0641

	PLA/PCL/PCL-*ran*-PC(s)					
T_c	$t_{50\% \text{ theo}}$ (min)	$t_{50\% \text{ exp}}$ (min)	n	K (min^{-n})	R^2	$1/t_{50\% \text{ exp}}$ (min^{-1})
124	13.160	13.417	2.93	3.64E-04	0.9999	0.0745
120	11.860	11.750	2.34	2.10E-03	0.9999	0.0851
116	11.017	10.184	2.09	4.56E-03	0.9999	0.0982
112	8.310	7.467	2.31	5.23E-03	0.9987	0.1339
108	8.466	7.734	2.26	5.51E-03	0.9991	0.1293
104	8.761	8.284	2.48	3.17E-03	0.9996	0.1207
100	10.953	10.200	2.37	2.37E-03	0.9995	0.0980
96	15.192	15.184	3.42	6.25E-05	0.9999	0.0659
92	20.181	17.950	3	8.32E-05	0.9955	0.0557

5. CONCLUSIONS

In this work, both melt and solution mixed 80/20 blends of PLA/PCL have been prepared in order to study the effect of the blending method on the crystallization behaviour of PLA. At the same time, in order to correlate the crystallization behaviour of PLA with PLA-PCL phases miscibility, poly(ε-caprolactone)-poly(carbonate) based copolymers, both block and random, have been tested as compatibilizers within the blends, by adding at 10% with respect to the minor phase.

Poly(ε-caprolactone)-poly(carbonate) based copolymers were synthetized by ring opening polymerization (ROP), using commercial ε-caprolactone and preformed poly(carbonate), and characterized by spectroscopic and thermal analyses.

The copolymers do not cause any effect on PLA/PCL phases miscibility, since no reduction of PCL particles and PLA T_g value has been detected in both melt and solution mixed blends. Therefore it is assumable that they do not migrate at the PLA-PCL interphase but are dispersed in one or both the phases.

At the same time copolymers addition causes a reduction of molecular weight in melt mixed blend. In particular, the random copolymer (PCL-*ran*-PC), characterized by a lower thermal stability than the block one (PCL-*b*-PC), causes a reduction of molecular weight from $\overline{M_n}$ =123 KDa to $\overline{M_n}$ =38 KDa during melt blending, whereas the same effect has not been detected in the corresponding solution mixed blends.

As result, PLA phase within melt mixed blends containing PCL-PC based copolymers has a higher tendency to crystallize during both isothermal and non-isothermal experiments. In particular, upon the addition of the random copolymer during melt blending (PLA/PCL/PCL-*ran*-PC(m)) an overall crystallization rate ten times higher than neat PLA (PLA(m)) has been detected, whereas no increase has been detected in the corresponding solution mixed blend PLA/PCL/PCL-*ran*-PC(s) (characterized by the same molecular weight of neat PLA). This effect has been attributed to an increase of the spherulitic growth rate due to the increase of chains mobility upon molecular weight reduction.

6. REFERENCES

1. Rosen SL. *Fundamental Principles of Polymeric Materials*.; 1993.

2. Tokiwa Y, Calabia BP, Ugwu CU, Aiba S. Biodegradability of plastics. *Int J Mol Sci*. 2009;10(9):3722-3742.

3. Lorenzo AT, Müller AJ. Estimation of the nucleation and crystal growth contributions to the overall crystallization energy barrier. *J Polym Sci Part B Polym Phys*. 2008;46(14):1478-1487.

4. Muthukumar M. *Nucleation in Polymer Crystallization*.; 2004.

5. Mandelkern L. Crystallization kinetics of homopolymers: bulk crystallization. *Crystallization of Polymers Volume 2*.; 2004:1-214.

6. Avrami M. Granulation, Phase Change, and Microstructure Kinetics of Phase Change. III. *J Chem Phys*. 1941;9(2):177-184.

7. Reddy MM, Vivekanandhan S, Misra M, Bhatia SK, Mohanty AK. Biobased plastics and bionanocomposites: Current status and future opportunities. *Prog Polym Sci*. 2013;38(10-11):1653-1689.

8. Philp JC, Ritchie RJ, Guy K. Biobased plastics in a bioeconomy. *Trends Biotechnol*. 2013;31(2):65-67.

9. Gandini A, Belgacem MN. Monomers, polymers and composites from renewable resources. 2008:401.

10. Gandini A, Lacerda TM, Carvalho AJF, Trovatti E. Progress of Polymers from Renewable Resources: Furans, Vegetable Oils, and Polysaccharides. *Chem Rev*. 2016;116(3):1637-1669.

11. Ulery BD, Nair LS, Laurencin CT. Biomedical applications of biodegradable polymers. *J Polym Sci Part B Polym Phys*. 2011;49(12):832-864.

12. Siracusa V, Rocculi P, Romani S, Rosa MD. Biodegradable polymers for food packaging: a review. *Trends Food Sci Technol*. 2008;19(12):634-643.

13. Auras R, Harte B, Selke S. An overview of polylactides as packaging materials. *Macromol Biosci*. 2004;4(9):835-864.

14. Narayanan N, Roychoudhury PK, Srivastava A. L (+) lactic acid fermentation and its product polymerization. *Electron J Biotechnol*. 2004;7(2):167-179.

15. Madhavan Nampoothiri K, Nair NR, John RP. An overview of the recent developments in polylactide (PLA) research. *Bioresour Technol*.

2010;101(22):8493-8501.

16. Hartmann MH. High Molecular Weight Polylactic Acid Polymers. *Biopolym from Renew Resour.* 1998:367-411.

17. Albertsson A-C, Varma IK. Recent Developments in Ring Opening Polymerization of Lactones for Biomedical Applications. *Biomacromolecules.* 2003;4(6):1466-1486.

18. Stanford MJ, Dove AP. Stereocontrolled ring-opening polymerization of lactide. *Chem Soc Rev.* 2010;39(2):486-494.

19. Kaihara S, Matsumura S, Mikos AG, Fisher JP. Synthesis of poly(L-lactide) and polyglycolide by ring-opening polymerization. *Nat Protoc.* 2007;2(11):2767-2771.

20. Avérous L. Polylactic Acid : Synthesis , Properties and Applications. *Synthesis (Stuttg).* 2008:2006-2008.

21. Saeidlou S, Huneault MA, Li H, Park CB. Poly(lactic acid) crystallization. *Prog Polym Sci.* 2012;37(12):1657-1677.

22. Chandra R, Rustgi R. Biodegradable polymers. *Prog Polym Sci.* 1998;23(7):1273-1335.

23. Vilaplana F, Strömberg E, Karlsson S. Environmental and resource aspects of sustainable biocomposites. *Polym Degrad Stab.* 2010;95(11):2147-2161.

24. Lim L-T, Auras R, Rubino M. Processing technologies for poly(lactic acid). *Prog Polym Sci.* 2008;33(8):820-852.

25. Södergård A, Stolt M. Properties of lactic acid based polymers and their correlation with composition. *Prog Polym Sci.* 2002;27(6):1123-1163.

26. Pantani R, De Santis F, Sorrentino A, De Maio F, Titomanlio G. Crystallization kinetics of virgin and processed poly(lactic acid). *Polym Degrad Stab.* 2010;95(7):1148-1159.

27. McNeill IC, Leiper HA. Degradation studies of some polyesters and polycarbonates-2. Polylactide: Degradation under isothermal conditions, thermal degradation mechanism and photolysis of the polymer. *Polym Degrad Stab.* 1985;11(4):309-326.

28. Nijssen B, Kamperman T, Jetten J. Acetaldehyde in mineral water stored in polyethylene terephthalate (PET) bottles: odour threshold and quantification. *Packag Technol Sci.* 1996;9(February):175-185.

29. Kawai T, Rahman N, Matsuba G, et al. Crystallization and melting behavior of poly (L-lactic acid). *Macromolecules*. 2007;40(26):9463-9469.

30. Cho TY, Strobl G. Temperature dependent variations in the lamellar structure of poly(l-lactide). *Polymer (Guildf)*. 2006;47(4):1036-1043.

31. Puiggali J, Ikada Y, Tsuji H, Cartier L, Okihara T, Lotz B. The frustrated structure of poly(l-lactide). *Polymer (Guildf)*. 2000;41(25):8921-8930.

32. Pracella M. Crystallization of Polymer Blends. *Handbook of Polymer Crystallization.*; 2013:287-325.

33. Dell'Erba R, Groeninckx G, Maglio G, Malinconico M, Migliozzi A. Immiscible polymer blends of semicrystalline biocompatible components: Thermal properties and phase morphology analysis of PLLA/PCL blends. *Polymer (Guildf)*. 2001;42(18):7831-7840.

34. Tsuji H, Tashiro K, Bouapao L, Narita J. Polyglycolide as a biodegradable nucleating agent for poly(L-lactide). *Macromol Mater Eng*. 2008;293(12):947-951.

35. Zhou J, Jiang Z, Wang Z, et al. Synthesis and characterization of triblock copolymer PLA-b-PBT-b-PLA and its effect on the crystallization of PLA. *RSC Adv*. 2013;3(40):18464.

36. Pan P, Shan G, Bao Y. Enhanced nucleation and crystallization of poly(L-lactic acid) by immiscible blending with poly(vinylidene fluoride). *Ind Eng Chem Res*. 2014;53(8):3148-3156.

37. Guo X, Liu H, Zhang J, Huang J. Effects of polyoxymethylene as a polymeric nucleating agent on the isothermal crystallization and visible transmittance of poly(lactic acid). *Ind Eng Chem Res*. 2014;53(43):16754-16762.

38. Detyothin S, Kathuria A, Jaruwattanayon W, Selke SEM, Auras R. Poly(Lactic Acid) Blends. In: *Poly(Lactic Acid): Synthesis, Structures, Properties, Processing, and Applications.*; 2010:227-271.

39. Goldberg D. A review of the biodegradability and utility of poly(caprolactone). *J Environ Polym Degrad*. 1995;3(2):61-67.

40. David DJ, Sincock TF. Estimation of miscibility of polymer blends using the solubility parameter concept. *Polymer (Guildf)*. 1992;33(21):4505-4514.

41. Koning, Duin, Pagnoulle, Jerome. Strategies for compatibilization of polymer blends. *Prog Polym Sci*. 1998;23(97):707-757.

42. Zeng J-B, Li K-A, Du A-K. Compatibilization strategies in poly(lactic acid)-based blends. *RSC Adv*. 2015;5(41):32546-32565.

43. Wu D, Zhang Y, Yuan L, Zhang M, Zhou W. Viscoelastic interfacial properties of compatibilized poly(ε-caprolactone)/polylactide blend. *J Polym Sci Part B Polym Phys*. 2010;48(7):756-765.

44. Na Y, He Y, Shuai X, Kikkawa Y, Doi Y. Compatibilization Effect of Poly(ε-caprolactone)-b-poly(ethylene glycol) block copolymers and phase morphology analysis in immiscible Poly(lactide)/Poly(ε-caprolactone) blends. 2002:1179-1186.

45. Rizzuto M, Marinetti L, Caretti D, Mugica A, Zubitur M, Müller AJ. Can Poly(ε-Caprolactone) crystals nucleate glassy Polylactide? *CrystEngComm*. 2017;19.

46. Choi N-S, Kim C-H, Cho KY, Park J-K. Morphology and hydrolysis of PCL/PLLA blends compatibilized with P(LLA-co-εCL) or P(LLA-b-εCL). *J Appl Polym Sci*. 2002;86(8):1892-1898.

47. Coleman MM, Serman CJ, Bhagwagar DE, Painter PC. A practical guide to polymer miscibility. *Polymer (Guildf)*. 1990;31(7):1187-1203.

48. Patrício T, Bártolo P. Thermal stability of PCL/PLA blends produced by physical blending process. *Procedia Eng*. 2013;59:292-297.

49. Patrício T, Domingos M, Gloria A, Bártolo P. Characterisation of PCL and PCL/PLA scaffolds for tissue engineering. *Procedia CIRP*. 2013;5:110-114.

50. Chen YY, Geever LM, Higginbotham CL, Devine DM. Analysis of the mechanical properties of solvent cast blends of PLA/PCL. *Eng Technol Res*. 2014;679:50-56.

51. Broz ME, VanderHart DL, Washburn NR. Structure and mechanical properties of poly(D,L-Lactic Acid)/poly(ε-Caprolactone). *Biomaterials*. 2003;24(23):4181-4190.

52. Fortelný I, Ostafińska A, Michálková D, Jůza J, Mikešová J, Šlouf M. Phase structure evolution during mixing and processing of poly(lactic acid)/polycaprolactone (PLA/PCL) blends. *Polym Bull*. 2015;72(11):2931-2947.

53. Simões CL, Viana JC, Cunha AM. Mechanical properties of poly(ε-caprolactone) and poly(lactic acid) blends. *J Appl Polym Sci*. 2009;112(1):345-352.

54. Urquijo J, Guerrica-Echevarría G, Eguiazábal JI. Melt processed PLA/PCL blends: Effect of processing method on phase structure, morphology, and mechanical properties. *J Appl Polym Sci*. 2015;42641(41):n/a-n/a.

55. Kim JK, Park DJ, Lee MS, Ihn KJ. Synthesis and crystallization behavior of poly(L-lactide)-block-poly(ε-caprolactone) copolymer. *Polymer (Guildf)*. 2001;42(17):7429-7441.

56. Dechy-Cabaret O, Martin-Vaca B, Bourissou D. Controlled ring-opening polymerization of lactide and glycolide. *Chem Rev*. 2004;104(12):6147-6176.

57. Cayuela J, Da Cruz-Boisson F, Michel A, Cassagnau P, Bounor-Legaré V. Synthesis of bisphenol-A polycarbonate-poly(ε-caprolactone) copolymers by reactive extrusion through in situ ε-caprolactone polymerization. 2016;104.

58. Müller AJ, Balsamo V, Arnal ML, Jakob T, Schmalz H, Abetz V. Homogeneous nucleation and fractionated crystallization in block copolymers. *Macromolecules*. 2002;35(8):3048-3058.

59. Carrasco F, Pagès P, Gàmez-Pérez J, Santana OO, Maspoch ML. Processing of poly(lactic acid): Characterization of chemical structure, thermal stability and mechanical properties. *Polym Degrad Stab*. 2010;95(2):116-125.